An overview on Global Positioning Techniques for Harsh Environments

CHAPTER 23

AN OVERVIEW ON GLOBAL POSITIONING TECHNIQUES FOR HARSH ENVIRONMENTS

Nicola Linty and Fabio Dovis
Politecnico di Torino, Italy

AU: Pls check. We have set affiliation as per style

AU: We have delete abstarct heading from here. PLS CHECK

THE SCOPE of this chapter is to present strategies and techniques used to increase the sensitivity of global navigation satellite system (GNSS) receivers in order to make them usable in harsh environments, such as urban canyons, light indoor scenarios, deep forests, or space. In such scenarios, the received signal experiences a lower signal-to-noise ratio, coupled with distortions and presence of spurious contributions, which affect the quality of the GNSS position, and sometimes even deny the positioning service. The chapter discusses the assistance that can be provided to the GNSS receiver through communication channels to ease the acquisition and tracking processes. Assisted GNSS is a consolidated standard, but other kinds of assistance and signal processing techniques can improve the ability of the receiver to process the signal at a low signal-to-noise ratio. The chapter introduces the common approaches to increase the sensitivity at the acquisition stage, discussing the impact on the accuracy of the delay and Doppler shift estimation, and the intrinsic limitation to coherent and noncoherent integration time extension. As far as the tracking stage is concerned, techniques to increase robustness to low signal-to-noise ratio scenarios are presented, considering the structure of new and modernized GNSS signals.

23.1 INTRODUCTION

Chapter 20 provides a general outline of the basic principles of global navigation satellite systems. It is worth recalling that the task of a GNSS receiver is to provide an estimate of the position, velocity, and time (PVT) of a user. This is achieved by

Handbook of Position Location: Theory, Practice, and Advances, Second Edition.
Edited by Seyed A. (Reza) Zekavat and R. Michael Buehrer.

Published 2019 by John Wiley & Sons, Inc.

processing radio frequency (RF) electro magnetic signals transmitted by a constellation of satellites by means of a specifically designed communication receiver. Briefly, their architecture is composed of a *physical layer* in charge of processing the received signal to detect and estimate some of its parameters, and by a *range layer* responsible for position computation [1–3]. Chapter 21 gives a detailed description of the digital signal processing techniques employed in a standard GNSS receiver physical layer. Such traditional acquisition and tracking schemes offer users satisfactory performance when the quality of the received signal is sufficiently high.

However, the rapid and widespread diffusion of GNSS for a large variety of location-based applications (LBAs) has pushed the performance requirements of GNSS receivers to extreme levels. Moreover, the present use of GNSS is rather different from its original conception. The global positioning system (GPS) was designed in the early 1970 by the Department of Defense (DoD) of the United States (US). Similarly, the GLObal NAvigation Satellite System (GLONASS) was developed by the Russian Federation. Both systems have been designed mainly for military applications: they were required to work outdoors, with a clear view of the sky and ideal line-of-sight conditions between the users and the satellites for most of the time. There were indeed no plans to use it in indoor environments. Furthermore, a start-up time of about one minute seemed to be adequate considering the maturity of the technology of the time. The size, cost and, in some cases, power consumption of such devices, were not primary drivers. Nowadays, thanks to the evolution of computational platforms, to the availability of more powerful processors, to the design of advanced signal processing techniques and, in parallel, to the spread of LBAs, GNSS is used by billions of people all around the world, and the number of civilian receivers outnumbers military devices by orders of magnitude. The purpose of GNSS has considerably changed: a GNSS receiver is nowadays required to work almost instantly, anywhere on the Earth, and to be small, cheap, and with low power consumption [4].

The need to use GNSS-based positioning also in environments where the signal-to-noise ratio is below the nominal level experienced in clear sky, and where the ideal propagation conditions are not fulfilled, led to the design of *high sensitivity* GNSS (HS-GNSS) receivers. High sensitivity receivers perform sophisticated signal processing operations in order to assure a PVT solution in those environments and situations in which a regular GNSS receiver would fail. Such scenarios include, but are not limited to, urban canyons, light indoor environments, deep forests, and space. The scope of this chapter is to present strategies and signal processing techniques used to increase the sensitivity of GNSS receivers in order to make them usable in such harsh environments.

At a high level, high sensitivity techniques involve two main strategies:

1. the increase of the signal processing gain by extending integration times, thus decreasing the minimum carrier-to-noise density power ratio (C/N_0) required for acquisition and tracking (i.e., increasing receiver sensitivity);
2. the use of GNSS assistance data (such as almanac, ephemeris, satellite health, GPS time and coarse user position) to assist and facilitate the receiver operations.

First, this introduction gives a general overview of high-sensitivity requirements. Then, in Section 23.2, the concepts of noise and correlation gain are described. These concepts are extended in Section 23.3, in which the two main strategies for increasing the sensitivity of a receiver are presented: the coherent and noncoherent integration time extension. Afterwards, Section 23.4 describes the consequences and drawbacks of the extension of the integration time and provides solutions; in particular, the problems of data bit transitions, Doppler shift, and Doppler rate are considered. In Section 23.5, the design and implementation of a high-sensitivity GNSS receiver is addressed, focusing on the acquisition and tracking stages. A few examples of acquisition and tracking results are also provided. Section 23.6 introduces the topic of GNSS assistance, which is of paramount importance when designing high-sensitivity receivers. Finally, Section 23.7 gives a brief overview of the advantages of the new and modernized GNSS signals as far as high sensitivity is concerned.

23.2 SIGNAL POWER, NOISE AND CORRELATION GAIN

One of the main features of any GNSS is the very low signal power received by the user (Chapter 20). GNSS signals are transmitted by a constellation of satellites, which are more than 20,000 km from the Earth. As an example, according to the GPS Interface Control Document (ICD) [5], the minimum received power level for the legacy GPS L1 C/A signal is equal to −158.1 dBW (assuming a unity gain right hand circularly polarized (RHCP) antenna [1]). Typical values for the noise are around −140 dBW, which means that the useful GNSS signal is completely buried in the noise floor. Multipath reflections, radio-frequency interference (RFI), obstacles, buildings, or additional propagation losses further affect the link budget. As an example, three layers of dry bricks or 20 cm of steel add an extra attenuation of about 30 dB. A more detailed analysis of the noise derivation is out of the scope of this chapter and can be found in Reference 4.

Chapter 21 (Section 21.1) carefully describes the GNSS received signal. In particular, the signal at the input of the signal processing blocks of a receiver (acquisition and tracking), denoted $y_{\mathrm{IF}}[n]$ and reported in Equation 23.1, is the sum of two different contributions:

- a *useful* signal component, $r_{\mathrm{IF}}[n]$, representative of the GNSS transmitted signal;
- a noise component, $w_{\mathrm{IF}}[n]$;

$$y_{\mathrm{IF}}[n] = r_{\mathrm{IF}}[n] + w_{\mathrm{IF}}[n]. \tag{23.1}$$

AU: Do you mean to say the "subscript" IF in reference the above equation? If not, the introduction of the IF acronym can be moved here

The subindex IF recalls the fact the the signal has been down-converted to an intermediate frequency (IF) by the receiver front-end. At this stage of the receiver, i.e., at the analog-to-digital converter (ADC) output, the signal is a sequence of samples taken at $t = nT_s$, where $T_s = 1/f_s$ and f_s is the sampling frequency. The notation $y_{\mathrm{IF}}[n]$ is then used to indicate the discrete-time signal, where $y_{\mathrm{IF}}(n) = y_{\mathrm{IF}}(nT_s)$ [6]. It has to be noted that only a single signal-in-space (SIS) contribution is considered, as

each single satellite signal can be separately received and processed thanks to the code division multiple access (CDMA) characteristics of GNSS signals. In other words, the intrasystem interference generated by other satellites of the constellation can be neglected.

AU: This acronym could be introduced upon first usage in the abstract as well

The signal-to-noise ratio (SNR) is commonly used in communications to characterized the noise contribution. It is defined as the ratio of the useful signal power to the noise power. Conversely, in GNSS the C/N_0 is used, being a quantity independent from the front-end filter bandwidth and thus from the receiver design (see Chapter 21, Section 21.2.2). The C/N_0 is defined as

$$C/N_0 = \frac{P_R}{N_0}, \tag{23.2}$$

where P_R is the signal power, evaluated on the whole signal bandwidth, and N_0 is the noise power density.

Considering legacy open GPS signals, in open-sky conditions, in absence of impairments and using a common antenna, the nominal value of the C/N_0 ranges between 45.5 and 55 dB-Hz [2]. Therefore, the typical sensitivity of a common GNSS receiver is around 45.5 dB-Hz. Typical values of C/N_0 for harsh environments are in the range 5 to 45.5 dB-Hz. The following classification is considered in the rest of this chapter:

- C/N_0 above the nominal value: $C/N_0 \geq 45.5$ dB-Hz. This is the case of "regular" open-sky signals, for which high sensitivity is not required.
- C/N_0 below the nominal value: 30 dB-Hz $\leq C/N_0 < 45.5$ dB-Hz. This is the case of weak signals, requiring high sensitivity receivers.
- Very low C/N_0: $C/N_0 < 30$ dB-Hz. This is the case of very weak signals, requiring advanced high-sensitivity techniques.

The SNR at the front-end output, denoted ρ_{IF}, can be derived by dividing the C/N_0 defined in Equation 23.2 by the front-end filter bandwidth B_{IF}:

$$\text{SNR} = \rho_{IF} = \frac{C/N_0}{B_{IF}} = \frac{P_R}{N_0 B_{IF}}. \tag{23.3}$$

A typical value of the bandwidth of a mass-market single frequency GPS receiver is 4 MHz. Thus, the resulting sensitivity of a common receiver in terms of SNR is –20.5 dB, while a high-sensitivity receiver is required to acquire signals down to –36 dB. A high-sensitivity professional receiver, with a bandwidth of 20 MHz, is able to acquire signals at a SNR as low as –43 dB.

23.2.1 The Correlation Gain

The first task of any GNSS receiver is to extract the signal from the noise floor in order to correctly detect and estimate the signal parameters. In the case of high-sensitivity receivers, this task is even harder. This is achieved by exploiting the CDMA structure of GNSS signals. The spreading codes used in GNSS are periodic sequences, modulated on top of the signal at a rate R_c. In the case of GPS L1 C/A,

$R_c = 1.023$ Mchip/s, and the code is 1023 chips long*. The length of the sequence, T_{code}, is then equal to

$$T_{\text{code}} = \frac{1023}{R_c} = \frac{1023}{1.023 \cdot 10^6} = 1 \text{ ms}. \tag{23.4}$$

The despreading is performed through the *correlation* operation. A portion of the received SIS is cross-correlated with a replica of the signal generated locally. Thanks to the excellent correlation properties of the spreading sequences used in GNSS, a correlation peak emerges in correspondence of the right delay between the received and local signals. The more evident and sharp the peak, the better the receiver performance. The ratio between the correlation peak and the correlation floor is the postcorrelation SNR. The longer the accumulation time within the correlation function, the higher the correlation peak, and therefore the higher the despreading gain that can be obtained.

Chapter 21 reports the expression of the postcorrelation SNR (Eq. 21.41):

$$\rho_a = \frac{P_R L}{N_0 B_{IF}} = \frac{C}{N_0} \frac{L}{2B_{IF}} = \rho_{IF} \frac{L}{2}. \tag{23.5}$$

$L/2$ is the correlation despreading gain. It is then determined by the term L, which corresponds to the number of samples of the incoming signal used to compute the correlation. Consequently, the product LT_s corresponds to the total length in time of the correlation procedure. LT_s is usually denoted *accumulation time*, *integration time*, or *predetection integration time*. In most implementations, LT_s is fixed to the length of a code period T_{code}, e.g., 1 ms for GPS L1 C/A legacy signals. In fact, when considering one full code period of the incoming signal and one full code period of the local signal, a complete correlation is performed.

In order to improve the despreading gain and, in turn, the postcorrelation SNR, different options can be considered:

- Increasing the sampling frequency f_s so as to increase the number of samples L. However, the correlated nature of adjacent noise samples leads to an increase of the noise contribution at the correlator output. This effect is magnified at high sampling frequencies [4].
- Using longer codes so as to increase the code period T_{code}. This is the case of modernized and new GNSS signals. For example, the code length of the Galileo E1b signal is four times the code length of the legacy GPS L1 C/A. Example 23.1 below demontrates such a gain.
- Extending the observation period of the incoming signal to more than one code period. This procedure is known as coherent integration time extension and is the core of high-sensitivity GNSS receivers.

Example 23.1: Extension of the Code Length

The goal of this example is to prove that a longer code benefits from a larger despreading gain, allowing the correct estimation of a peak even in the presence of a high noise standard deviation.

*Parameters for other signals can be found in Chapter 20 and in Section 23.7

In Examples 21.1 and 21.2, the cross-correlation of a code is evaluated, respectively, in the absence and in the presence of noise. A 20-chip long code is considered:

$$c_{\text{loc}} = \sum_{i=0}^{19} \alpha_i r(t - iT_c). \tag{23.6}$$

Similarly, a 31-chip-long code can be defined:

$$d_{\text{loc}} = \sum_{i=0}^{29} \beta_i r(t - iT_c), \tag{23.7}$$

where

- $\mathrm{r}\beta_i = [1\ 1\ -1\ 1\ -1\ 1\ 1\ -1\ -1\ 1\ 1\ 1\ 1\ 1\ -1\ -1\ \ldots$
  $-1\ 1\ 1\ -1\ 1\ 1\ 1\ -1\ 1\ -1\ 1\ -1\ -1\ -1\ -1]$;
- $r(t)$ is the unitary amplitude rectangular function; and
- T_c is the chip length, the inverse of the code rate $R_c = 0.5$ MHz.

The tasks to be performed are:

1. generate the incoming signals, c_{in} and d_{in}, composed by three periods of c_{loc} and d_{loc}.
2. sample the incoming and local codes at $f_s = 8$ MHz, obtaining the sequences of samples $c_{\text{in}}[n]$, $c_{\text{loc}}[m]$, $d_{\text{in}}[n]$, and $d_{\text{loc}}[m]$, with $n = 1,\ldots,N$ and $M = 1,\ldots,3N$, and $N = 20(f_s/R_c)$;
3. generate three realizations of additive white Gaussian noise (AWGN) noise $w[n]$, with standard deviation equal to 1, 4, and 8 respectively, and sum them to the incoming signal:

$$s[n] = c_{in}[n] + w[n], \tag{23.8}$$

$$r[n] = d_{in}[n] + w[n], \tag{23.9}$$

   with $n = 1,\ldots,N$;
4. plot the correlation function, where the initial code phase of $c_{\text{in}}[n]$ and $d_{\text{in}}[n]$ is equal to 4 chips, and for the different values of the noise standard deviation;
5. compare the results in terms of peak detection.

Solution

Figure 23.1 shows the results when considering a 20-chip-long input code. As in the example reported in Chapter 21, the the correlation peak is clearly visible when the noise variance is equal to 1. When increasing the noise variance to 4, the correlation peak is still visible, but the noise floor is larger and an error of a few fractions of a chip is introduced. On the contrary, for higher noise variances, such as eight, the peak is buried in the noise floor, and the peak estimation procedure fails.

As expected, a longer code gives a larger correlations gain. Figure 23.2 reports the same correlation results as above, obtained using a 31-chip-long code. The correlation peak is correctly estimated also for a noise variance of eight. In addition,

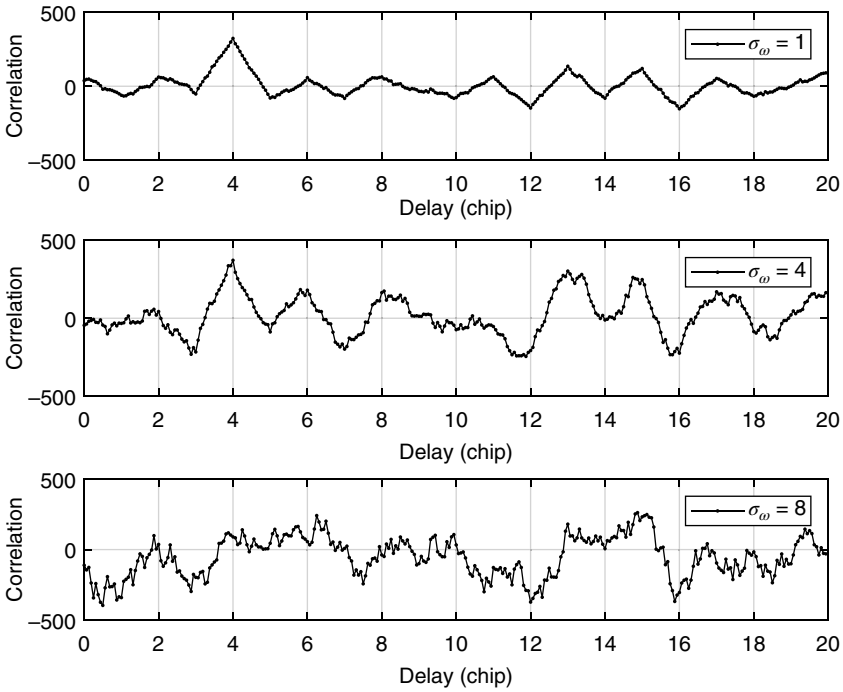

Figure 23.1 Correlation peak for a 20-chip-long sequence and for different values of the noise variance.

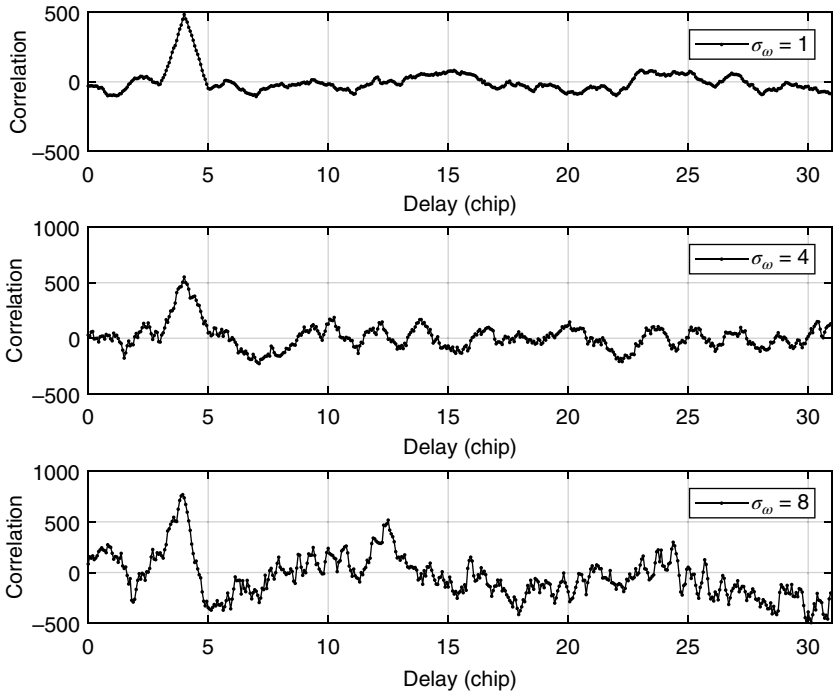

Figure 23.2 Correlation peak for a 31-chip-long sequence and for different values of the noise variance.

the ratio between the peak and the noise floor (postcorrelation SNR) is higher, thus improving the detection performance.

23.3 INTEGRATION TIME EXTENSION

In Chapter 21.3.2 the concept of the cross ambiguity function (CAF) is defined. The CAF (Eq. 21.38) is the squared envelope of the correlations evaluated in the search space (SS) domain:

$$S_{y,r}\left(\overline{\tau},\overline{f}_D\right)=\left|\frac{1}{L}\sum_{n=0}^{L-1}y_{\mathrm{IF}}[n]\,c_b\left(nT_s-\overline{\tau}\right)e^{j2\pi\left(f_{\mathrm{IF}}+\overline{f}_D\right)nT_s}\right|^2, \tag{23.10}$$

where:

- $S_{y,r}$ is the CAF;
- $\overline{\tau}$ and $\overline{f}_D$ are the values of the code delay and of Doppler frequency under evaluation, and they define the SS;
- $y_{\mathrm{IF}}[n]$ is the received GNSS SIS;
- $c_b(nT_s-\overline{\tau})$ is the local code, generated with a code delay equal to $\overline{\tau}$.
- $e^{j2\pi(f_{\mathrm{IF}}+\overline{f}_D)nT_s}$ is the local carrier, generated with a Doppler frequency shift equal to $\overline{f}_D$.

It must be remarked that the noise samples $w[n]$ in the received signal have an effect on each cell of the SS, altering the result in the CAF evaluation. Such noise contribution must be reduced. The noise can be modelled as a zero-mean AWGN random process; therefore averaging operations can reduce its impact. As explained in Section 23.2, averaging can be obtained by increasing the number of samples of the incoming signal used in the CAF evaluation. Recalling the expression of the CAF, this can be done before or after the envelope operation, leading to the two dominant strategies for integration time extension: *coherent* and *noncoherent* integration.

23.3.1 Coherent Integration Time Extension

In the first case, averaging is performed before the envelope operation. This approach is equivalent to increasing the value of L. N_c coherent sums can be performed in the CAF evaluation, thus leading to an integration time equal to:

$$T_c=N_c\cdot LT_s. \tag{23.11}$$

As the averaging operation is performed before the modulus square operation, it is referred to as coherent integration, and T_c is called *coherent integration time*.

The expression of the CAF the becomes:

$$\begin{aligned}S_{y,r,c}\left(\overline{\tau},\overline{f}_D\right)&=\left|\frac{1}{N_c}\sum_{m=0}^{N_c}\left(\frac{1}{L}\sum_{n=0}^{L-1}y_{\mathrm{IF}}[n]\,c_b\left(nT_s-\overline{\tau}\right)e^{j2\pi\left(f_{\mathrm{IF}}+\overline{f}_D\right)nT_s}\right)\right|^2\\&=\left|\frac{1}{N_cL}\sum_{n=0}^{N_cL-1}y_{\mathrm{IF}}[n]\,c_b\left(nT_s-\overline{\tau}\right)e^{j2\pi\left(f_{\mathrm{IF}}+\overline{f}_D\right)nT_s}\right|^2.\end{aligned} \tag{23.12}$$

The advantage of coherent summations is that the signal power is increased by a factor proportional to N_c, while the noise power is constant, as long as noise is zero mean, white, and Gaussian. Therefore, the postcorrelation SNR increases by a factor N_c. For instance, if coherent summation over two code periods is carried out ($N_c = 2$), the SNR increases by a factor of two, corresponding to about 3 dB. The derivation of the noise variance and of the theoretical distributions is provided in Section 23.5.1.

As a quality metric of the GNSS signal at the acquisition stage, the coherent output SNR is considered, and under ideal conditions (infinite front-end filter bandwidth and no quantization and frequency mismatching loss) it can be defined as

$$\rho_c = \frac{C}{N_0}\frac{LN_c}{2B_{IF}} = \rho_{IF}\frac{LN_c}{2} = \rho_\alpha N_c, \tag{23.13}$$

where ρ_{IF} is the SNR at the acquisition input, defined in Equation 23.3. The term $LN_c/2$ accounts for both the despreading gain $L/2$ and the gain of the coherent integration (N_c) contributions. However, in real conditions, the front-end filtering effect leads to a nonnegligible loss in the achievable coherent gain, since the pseudorandom noise (PRN) code cannot be considered a pure square wave, thus impacting the shape of the correlation peak, which appears rounded. Additional losses to the coherent SNR, such as quantization effect, code alignment, and frequency mismatch are deeply addressed in Reference 4.

The longer the coherent integration time is, the lower the noise floor will be, and the better the detection of the CAF peak will be. However, there are several limits in the extension of the predetection integration time, as clarified in Section 23.4. To overcome these issues, noncoherent accumulations can be performed.

Example 23.2: Extension of Integration Time

In Example 23.1, cross-correlation of a code in the presence of noise is evaluated, respectively, for a short and for a long sequence, proving that long sequences guarantee a larger despreading gain.

The goal of this example is to prove that a correlation gain can be obtained also by extending the integration time. The tasks to be performed are

1. generate the incoming signals, c_{in}, composed by 20 periods of c_{loc};
2. sample the incoming and local codes at $f_s = 8$ MHz, obtaining the sequences of samples $c_{\text{in}}[n]$ and $c_{\text{loc}}[m]$, with $n = 1,\ldots,N$ and $M = 1,\ldots,20N$, and $N = 20(f_S/R_c)$;
3. generate three realizations of AWGN $w[n]$, with standard deviation equal to 1 and 12.5, respectively, and sum them to the incoming signal:

$$s[n] = c_{\text{in}}[n] + w[n], \tag{23.14}$$

   with $n = 1,\ldots,N$;
4. generate the correlation for 10 subsequent portions of the incoming signal and sum them;

5. plot the correlation function, where the initial code phase of $c_{\text{in}}[n]$ and $d_{\text{in}}[n]$ is equal to 4 chips, and for the different values of the noise standard deviation;
6. compare the results in terms of peak detection.

Solution

Figure 23.3 reports the correlation results for the standard case ($N_c = 1$), as shown in Example 21.2, and for the case $N_c = 10$. As expected, in the second case it is possible to correctly detect the correlation peak at the right delay of 4 chips. Larger values of N_c allow detection of the correlation peak also for higher values of the noise variance.

23.3.2 Noncoherent Integration Time Extension

An averaging operation can be performed also after the envelope. N_n noncoherent sums are performed in the CAF evaluation, thus leading to an overall integration time equal to:

$$T_{nc} = N_n \cdot T_c = N_n \cdot N_c \cdot LT_s. \tag{23.15}$$

This kind of operation is denoted noncoherent integration, as the phase of the signal is lost in the square operation. T_{nc} is called *noncoherent integration time*.

The expression of the CAF then becomes:

$$S_{y,r,n}\left(\overline{\tau}, \overline{f}_D\right) = \frac{1}{N_n}\sum_{p=1}^{N_n}\left|\frac{1}{N_c}\sum_{m=1}^{N_c}\left(\frac{1}{L}\sum_{n=0}^{L-1} y_{\text{IF}}[n]c_b(nT_s - \overline{\tau})e^{j2\pi(f_{\text{IF}}+\overline{f}_D)nT_s}\right)\right|^2. \tag{23.16}$$

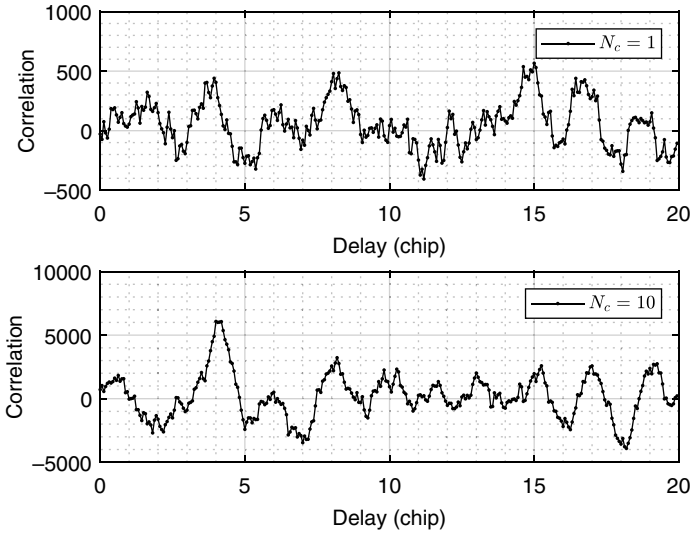

Figure 23.3 Correlation peak for different values of the integration time (N_c sums).

In this case, each block of $N_n N_c L$ samples is not treated as a single block but rather split into N_n sub-blocks, which are separately processed. Noncoherent accumulations are obtained summing noncoherently several instances of coherent integration. This strategy improves the capabilities of detecting weaker signals, at the expense of an increased number of operations.

It has to be noted that the Doppler frequency shift has to be taken into account when the coherent results are summed together. In the acquisition process, the Doppler effect on the spreading code is normally neglected. Therefore, the initial phase of the incoming code can change slightly with respect to the locally generated sequence, depending on the absolute value of the Doppler shift. In order to compensate for this, the coherent correlations need to be properly time-shifted during the noncoherent accumulation process.

When performing the summation after the envelope, both the signal and the noise power are increased. The theoretical distributions are provided in Section 23.5.1. The signal increases by a factor N_n, while the noise increases by a factor $\sqrt{N_n}$ [4]. For instance, if a noncoherent summation over two code periods is carried out ($N_n = 2$), the signal power increases by a factor of two and the noise by a factor of $\sqrt{2}$. This is due to the fact that the noise after the envelope is no longer zero mean. Therefore, the postcorrelation SNR increases by a factor of $2/\sqrt{2} = \sqrt{2}$, corresponding to about 1.5 dB. This is known as *squaring loss* [7].

An equivalent coherent SNR can be defined as the coherent SNR required for a noncoherent detector based on N_n accumulations in order to achieve the same performance of a pure coherent detection. The equivalent SNR can be defined as

$$\rho_n\big|_{\mathrm{dB}} = \rho_c\big|_{\mathrm{dB}} - L_s + 10\log_{10} N_n, \tag{23.17}$$

where L_s is the squaring loss. Analytical derivation for the squaring loss can be found in References 4 and 8.

Given a target scenario, in terms of sensitivity, signal dynamic, and availability of assistance information, a trade-off between the coherent integration time and the number of noncoherent accumulations has to be analyzed. In absence of other issues, which will be considered in Section 23.4, coherent integration is more efficient than noncoherent integration in terms of SNR gain, and thus preferable. Being the extension of the coherent integration time limited by several factors, as detailed later on, noncoherent accumulations are exploited to further increase the SNR gain.

Figure 23.4 summarizes the concept of coherent and noncoherent integration.

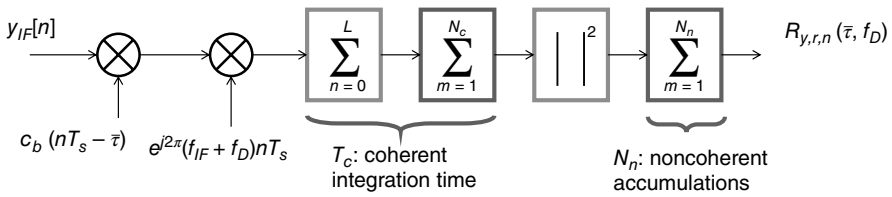

Figure 23.4 Coherent and noncoherent integrations.

23.3.3 Differential Combination

Although being much less common in consumer receivers, differential combination can be included into the high sensitivity techniques. It was first proposed by References 9 and 10. Differential correlation can be seen as an extension of noncoherent intregration, in which, before the square envelope operation, the correlation output is multiplied by the conjugate of the correlation output obtained at the previous integration interval and accumulated. Denoting the $R[m]$ the correlation output at epoch m,

$$R[m] = \frac{1}{L}\sum_{n=0}^{L-1} y_{\mathrm{IF}}[n]\, c_b(nT_s - \overline{\tau})\, e^{j2\pi\left(f_{\mathrm{IF}} + \overline{f}_D\right)nT_s}, \tag{23.18}$$

the differential combination integration assumes the form

$$S_{y,r,d} = \left|\sum_{m=2}^{M} R[m]R^*[m-1]\right|^2. \tag{23.19}$$

A slight performance improvement can be obtained when compared to noncoherent integration, because the signal components remain highly correlated in two consecutive correlation intervals, whereas the noise components tends to be decorrelated. A second advantage is the computational burden required, due to the fact that the SS size does not change, as described in Reference 11. However, the despreading gain is lower than the gain achievable exploiting a pure coherent integration scheme. Furthermore, it suffers from the phase reversal due to bit transition. Advanced and generalized differential combination techniques have been studied, and a summary is reported in Reference 12.

23.4 EFFECTS OF INCREASED INTEGRATION TIME

The integration time extension is the natural and straightforward solution to increase the receiver sensitivity. However, integration time extension introduces new issues, and high-sensitivity GNSS receivers are required to tackle several problems. The main issues are described in detail hereafter.

23.4.1 Data Transition

Most of the GNSS signals, such as GPS L1 C/A and Galileo E1b, are modulated by a navigation message. The navigation message is transmitted at a lower rate with respect to the spreading code and contains important information used in the PVT computation. The presence of navigation data is an additional obstacle when dealing with denied environments, for different reasons:

- navigation data demodulation cannot be achieved due to high bit error rate (BER) when processing very feeble GNSS signals (e.g., below 24 dB-Hz for GPS legacy signals) [3];

- at low C/N_0 also the data bit synchronizing could fail, thus preventing the generation of pseudoranges;
- the data bit length T_b limits the coherent integration time extension, since data bit transitions introduce shifts in the carrier phase within the integration window, leading to partial or total cancellation of the correlation power.

In Section 23.3 we described how extending the coherent integration time can improve the postcorrelation SNR. However, this is valid as long as no phase transitions due to the navigation message bits occur.

Figure 23.5 depicts a standard GNSS receiver acquisition stage, in which GPS L1 C/A signals are considered. The code period is $T_{\text{code}} = 1$ ms and the data bit duration is $T_b = 20$ ms. The navigation message bits, the SIS received code, and the local code are drawn, respectively, in green, blue, and red. The correlation between 1 ms of received signal and 1 ms of local code does not include a bit transition. As a result, the monodimensional CAF depicted in the figure exhibits a clear correlation peak.

When extending the integration time, for instance to $T_c = 10$ ms, two situations might occur. If we are lucky enough, no data bit transition will occur within the integration period. This happens if the 10 ms are entirely included in the same bit of the navigation message, of if they are across two bits with the same sign. Also in this case, no side effects occur. The first situation is depicted in Figure 23.6. $N_c = 10$ code periods of the incoming signal are coherently accumulated and correlated with

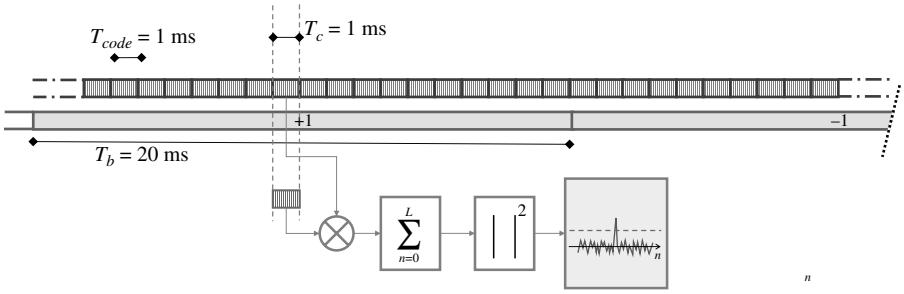

Figure 23.5 Pictorial representation of the correlation procedure in the case $T_c = 1$ ms.

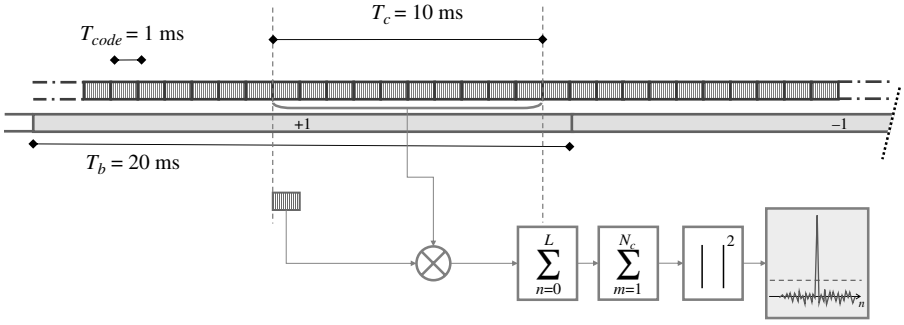

Figure 23.6 Pictorial representation of the correlation procedure in the case $T_c = 10$ ms.

the local code. The CAF peak is clear and higher than in the previous case because of the coherent integration gain. The CAF can be envisaged as the sum of 10 CAFs, each of them containing a positive correlation peak similar to the one in Figure 23.5.

On the contrary, if a data transition occurs within the coherent integration integration period, the signal detection might fail. The example reported in Figure 23.7 shows the worst case, i.e., the case in which a bit transition falls exactly in the middle of the coherent integration period. The correlation peak is absent, because the phase transition induced by the −1 bit annihilates the correlation. The resulting CAF can be envisaged as the sum of 10 correlations, 5 of them containing a positive peak and 5 of them containing a negative peak. Intermediate conditions can occur, leading to similar results.

This last example shows why the bit duration poses a severe limit to the integration time extension. In order to avoid correlation cancellation, it is required to have $T_c \leq T_b$, which means that the coherent integration time is limited to 20 ms for GPS L1 C/A signals.

It has to be reminded that navigation message bit synchronization has to also be achieved to avoid correlation losses. The time instant in which the navigation bit transition occurs has to be known by the receiver. This is normally the case in the tracking stage, but it never happens for acquisition, unless some aiding is provided. To minimize the probability of correlation annihilation due to bit transition, a common solution is to limit the coherent integration time to half the bit length, i.e., $T_c = 10$ ms. To further reduce this probability, it is also possible to perform two acquisition trials, using two consecutive 10-ms-long sequences. This assures that at least in one of the two CAFs no transitions occurred.

In order to overcome the data transition problem, several solutions are possible:

- the use of pilot dataless signals, such as Galileo E1c, as described in Section 23.7.2;
- the use noncoherent sums, as described in Section 23.3.2;
- the wipe-off of the navigation message, exploiting assistance information, as described in Section 23.4.1;
- the prediction of the navigation message data bits, as detailed in Section 23.4.1.

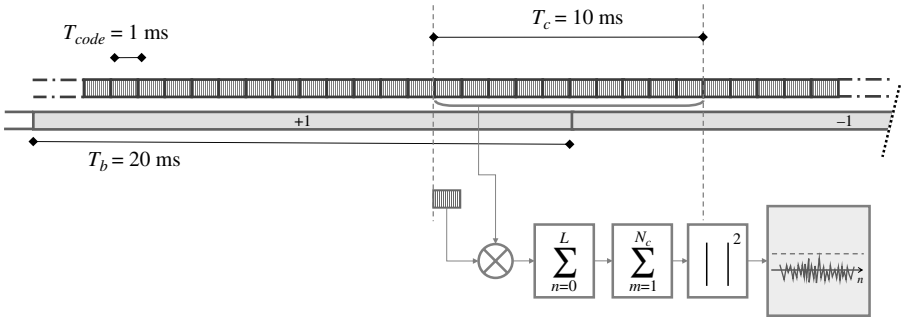

Figure 23.7 Pictorial representation of the correlation procedure in the case $T_c = 10$ ms, and a bit transition occurs at half the integration period.

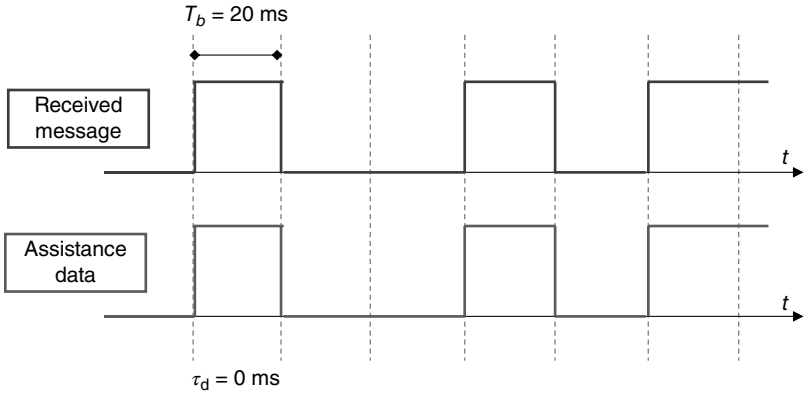

Figure 23.8 Perfect data wipe-off.

Navigation Message Wipe-Off The bits of the navigation message can be wiped-off, assuming that:

1. the sequence of bits is known;
2. precise time information to synchronize the wipe-off operation is available.

The stream of data bits is normally included in the information of Assisted GNSS (A-GNSS). Reference stations are able to predict the content of the message and to send it to enabled receivers. In this way, on one side the receiver does not have to demodulate the message, as all the information needed for the PVT computation are provided by A-GNSS. On the other side, an ideally perfect navigation message wipe-off can be performed on the SIS, allowing arbitrarily long coherent integration times.

The navigation data bits can also be provided by a reference receiver, located close to the high-sensitivity receiver, as is normally done in geodesy. Also peer-to-peer and cooperative networks can be exploited, as described in Reference 13.

When the accuracy time information is limited, an additional correlation loss is introduced. In Reference 14, a set of semi-analytical simulations, emulating different levels of timing accuracy, has been performed to assess the impact of the assistance timing error. A simulated GPS L1 C/A signal, characterized by a data bit transition every 20 ms is considered. Coherent integration at $T_c = 20$ ms is performed on the input signal. An A-GNSS assistance system is emulated: the sequence of bits is assumed always correct, while a delay τ_d in the range 0 to 10 ms, is artificially introduced. As expected, in the ideal case of $\tau_d = 0$ ms the wipe-off is perfect. Figure 23.8 depicts this situation: the incoming data bits and the assistance message are perfectly synchronized. Consequently, all the signal power contributes to the correlation peak.

On the contrary, when an error τ is present, part of the power of the correlation operation is lost, as shown in Figure 23.9, where $\tau \simeq 4$ ms. The worst case is when the bit transition happens exactly at half the bit length, which is for $\tau_d = 10$ ms; in this case, the phase change completely cancels the correlation result.

Figure 23.10 depicts the correlation SNR during a simulation for different values of the assistance timing error and for different values of signal C/N_0, confirming the theoretical assumptions. As long as the timing error increases, both the magnitude of

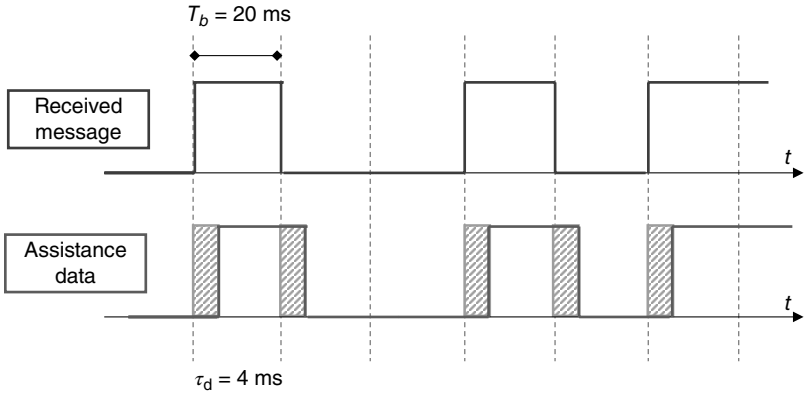

Figure 23.9 Data wipe-off in the case of an error in the time synchronization.

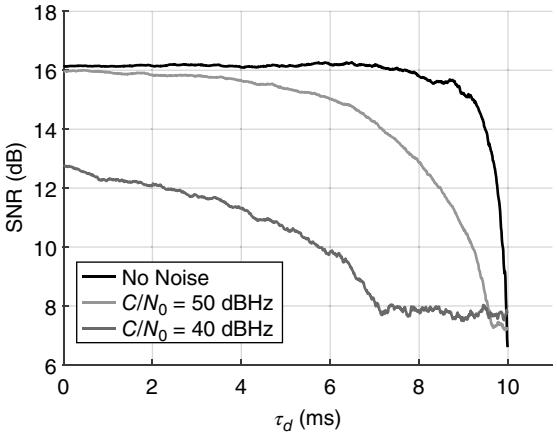

Figure 23.10 Correlation peak magnitude versus assistance timing error.

the peak and the noise floor level decease, with different trends. In the ideal case (no noise, black line), the SNR is constant until an error of about 8 ms; after this value the SNR starts falling to zero. On the contrary, for real signals, with C/N_0 equal to 50 and 40 dB-Hz, respectively, the SNR decreases much faster as long as the error increases. In the latter case, an error equal to 7 ms already completely cancels out the correlation. After this value, the correlation peak is completely buried in the noise floor.

Data Bits Prediction and Estimation As an alternative, data bits can be predicted or estimated.

In the first case, it is possible to foresee the incoming navigation message bits by exploiting the regular structure of the navigation message. For instance, the preamble, once determined for the first time, is always identical. Similarly, in the case of GPS legacy signals, ephemeris and clock parameters are updated every 2 hours, while the almanac is updated at least every 6 days. The correspondence bits can thus can be propagated from a frame to the following one. Furthermore, some information common to all GNSS satellites can be demodulated from the signals with high C/N_0

TABLE 23.1 Length of the Data Bit for the Most Common OS Navigation Signal.

Signal	T_b
GPS L1 C/A	20 ms
GPS L1C	10 ms
GPS L2C	20 ms
GPS L5 I	10 ms
GPS L5 Q	dataless
Galileo E1b	4 ms
Galileo E1c	dataless
Galileo E5A-I	20 ms
Galileo E5A-Q	dataless
Galileo E5B-I	4 ms
Galileo E5B-Q	dataless

and exploited to increase the coherent integration time for low power signals. This makes the overall navigation message partially deterministic.

A second possibility is offered by estimation techniques. The most simple algorithm consists in trying all the possible combination of bits and then choosing the one offering the highest postcorrelation SNR. However, this is possible only if bit synchronization has already been achieved. The main drawback is the exponential increase of the computational complexity.

23.4.2 Secondary Code Synchronization

Modernized and new GNSS signals contain a secondary code in addition to the primary code. For example, in the case of Galileo E1c, the code is tiered to the primary code, 25 chips long, thus spanning a total time of 100 ms. The sequence is known and periodic; however, it must be wiped off from the signal in order to extend the integraion time. Synchronization must be achieved, leading to an increased dimension of the SS in the code delay domain and thus to a worsening of the targeted false alarm probability of the overall acquisition system, as shown in Reference 15.

The secondary code can be removed either through self-techniques, such as maximum likelihood estimator (MLE) techniques, or exploiting assistance data. However, such techniques are not optimal at low C/N_0.

More details about high-sensitivity techniques for new and modernized GNSS signals are reported in Section 23.7.

23.4.3 Considerations on the Doppler Frequency

A complete description and derivation of the Doppler frequency affecting a GNSS signal has been provided in Chapter 21. The Doppler frequency at the receiver is caused by the combination of three different factors: the motion of the satellite, the motion of the user, and any uncompensated frequency offset in the receiver reference oscillator.

Good high sensitivity performance can be achieved only if the user dynamics are limited. The optimal situation is when the receiver is stationary or moving at relatively low constant velocity or very low acceleration, so that the only contribution of the Doppler shift is due to the satellites' motion.

During their pass, GPS satellites are moving toward and away from a static receiver on the Earth surface. They reach the maximum relative speed during rising and setting, when they are at zero elevation. For GPS satellites' orbit, $v_{max} = 930$ m/s. The maximum Doppler frequency is then equal to

$$f_{D,\max} = \frac{f_{L1} \cdot v_{\max}}{c} = \frac{1575.42 \times 10^6 \cdot 930}{c} = 4.9 \text{ kHz}, \tag{23.20}$$

where c is the speed of light. Similarly, the minimum Doppler frequency is equal to –4.9 kHz. Therefore, the Doppler range to be evaluated amounts to

$$\delta f = f_{D,\max} + |f_{D,\min}| = 9.8 \text{ kHz}. \tag{23.21}$$

For terrestrial applications, receiver motion is very small compared to the satellite speeds, so its effect is normally negligible. There is up to approximately 1.5 Hz of Doppler frequency for each 1 km/h of receiver speed [4]. Nevertheless, for high-sensitivity receivers featuring long integration times this should be considered.

For space applications, the relative speed between receiver and satellite can increase a lot, as described in Reference 16. Therefore, the maximum Doppler frequency can reach values as high as 20 kHz, and $\delta f = 40$ kHz. The main problem to face with such a large SS is that the number of frequency bins to be evaluated in the SS significantly increases, thus raising the acquisition time.

The total number of bins N_{bin} to be evaluated in the Doppler domain search depends indeed on the size of the SS and on width of the frequency bin:

$$N_{\text{bin}} = \left\lceil \frac{\delta f}{\Delta f} \right\rceil + 1. \tag{23.22}$$

The size of a Doppler bin Δf depends in turn on the coherent integration time, taking into account the *mistuning loss*. Chapter 21.3.2 (Fig. 21.7) describes the topic in detail and gives the following empirical rule to minimize the losses:

$$\Delta f = \frac{2}{3T_c}. \tag{23.23}$$

The correlation peak in frequency domain varies with frequency as a sinc function, as depicted in Figure 23.11. A larger T_c improves the sensitivity, but increases the width of the sinc function. If T_c is doubled, then sinc function width is halved and the number of frequency bins is doubled. It should be noted that, while a mistuning loss of a few dBs can be acceptable when working with signals at a nominal C/N_0, in the case of a high-sensitivity receiver the value of Δf might be further lowered to reduce the loss [3].

For large values of the integration times, Δf becomes extremely low. As an example, a coherent integration time equal to 3 s leads to a value of $\Delta f = 0.22$ Hz. Even though the Doppler resolution improves, the number of bins to be evaluated

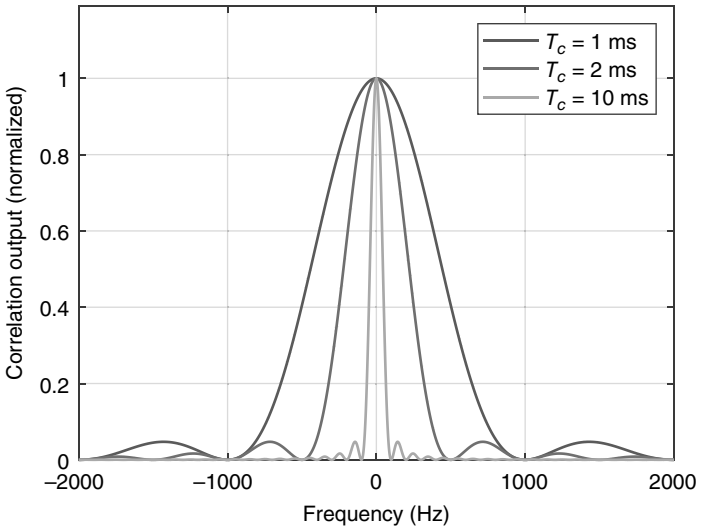

Figure 23.11 Correlation peak in the frequency domain for various values of T_c.

in the Doppler domain search excessively increases. Considering a Doppler range $\delta f = 9.8$ kHz, the value of N_{bin} is approximately 44,000, which is a nonreasonable value for terrestrial GNSS applications. In space environment, due to a wider Doppler range domain, the issue is magnified.

In a fast fourier transform (FFT)-based acquisition scheme parallel in time domain, the time required for the CAF computation depends on the number of frequency bins and on the overall observation time. It is called mean acquisition time (MAT), and it is expressed as:

$$T_a = T_c \cdot N_n \cdot N_{\text{bin}}. \tag{23.24}$$

This has clearly an impact in both the computational burden of the receiver and the time to first fix (TTFF). TTFF is defined as the time a receiver need from the moment it is switched on to the moment it provides the first PVT solution, and it depends on size of the SS, on the detection probability, on the probability of false alarm, and on the integration time.

Large banks of correlators or advanced digital signal processing operations are required to maintain an affordable MAT. Alternatively, it is necessary to reduce the frequency SS range by exploiting some sort of Doppler frequency aiding, such as assistance information, or relying on integration with other sensors. Even if a precise Doppler frequency is available the code alignment requires an accurate timing synchronization, better than 1 ms. An example is reported in Section 23.6.1.

23.4.4 Clock Errors and Stability

It should be mentioned that, even in presence of high accurate Doppler aiding, residual Doppler may be still present due to the finite accuracy of the local oscillator frequency, which usually differs from the nominal value by an amount related to the

adopted oscillator technology. Moreover, significantly longer integration intervals also require a very stable receiver oscillator. When computing the total frequency range uncertainty of the unknown frequency offset, an additional 1.575 kHz for each 1 ppm of unknown receiver oscillator offset has to be considered.

Typical figures of (relative) frequency accuracy are 10^{-6} for temperature compensated crystal oscillators (TCXOs) and 10^{-8} for oven controlled crystal oscillators (OCXOs). Improved performances can be attained by using atomic clocks (frequency stability up to 10^{-26}). However, cost, size, and power consumption of these types of oscillators limits their use for commercial applications.

23.4.5. Impact of Doppler Rate

Standard GNSS receivers tracking architectures are based on the assumption that the maximum change in the signal Doppler frequency is small when compared to the inverse of the integration time. The impact of Doppler rate is typically considered negligible, and the Doppler frequency is assumed constant over a single measurement epoch [17]. In fact, the magnitude of rate of change of a GNSS satellite's relative Doppler frequency is usually relatively small, if compared to the Doppler itself. For a static user, considering GPS and Galileo legacy signal in L1, it can increase up to 0.8 Hz/s depending on the satellite elevation and on the user's latitude [4]. However, when either the receiver velocity or the integration time significantly increase, the satellite Doppler rate becomes potentially significant, and the sole knowledge of the instantaneous Doppler might be not sufficient. The capability of providing the GNSS receiver with an accurate Doppler rate aiding allows the local carrier generator to follow the Doppler variation over time, thus making the receiver more robust to the high dynamic.

Requirements of such an aiding, in terms of accuracy, have to be assessed while taking into account the coherent integration time adopted at the acquisition stage, which determines the CAF resolution Δf. As an example, supposing that the receiver is provided with an ideal estimate of the Doppler frequency and an accurate Doppler rate aiding, the required accuracy of the Doppler rate estimate has to be such that the final mismatching between the true average Doppler frequency and the estimated average Doppler frequency during the overall acquisition period lies within half of the CAF resolution. Figure 23.12 shows the theoretical frequency mismatching between the average estimated Doppler frequency and the true average Doppler frequency in the case of very weak GPS (left plot) and Galileo (right plot) signal acquisition at 10 dB-Hz for different values of the Doppler rate bias, which is the shift between the true Doppler rate affecting the GNSS signal and the Doppler rate estimate from the aiding source.

Unmodelled receiver velocity introduces a further component in the relative Doppler and Doppler rate. Any 19 cm movement (i.e., the wavelength at L1) in the direction of a satellite induces an unexpected Doppler rate and introduces a phase shift through 360°, leading to signal annihilation. Figure 23.13 shows the value of the coherent integration time for which a complete phase shift occurs, for any velocity from 0 to 2 m/s. Receiver velocities up to 2 m/s (typical pedestrian velocity) can already annihilate the signal for an integration time of 100 ms. When it is increased to 1 s, the unmodelled velocity should be lower than 0.2 m/s to keep tracking the SIS.

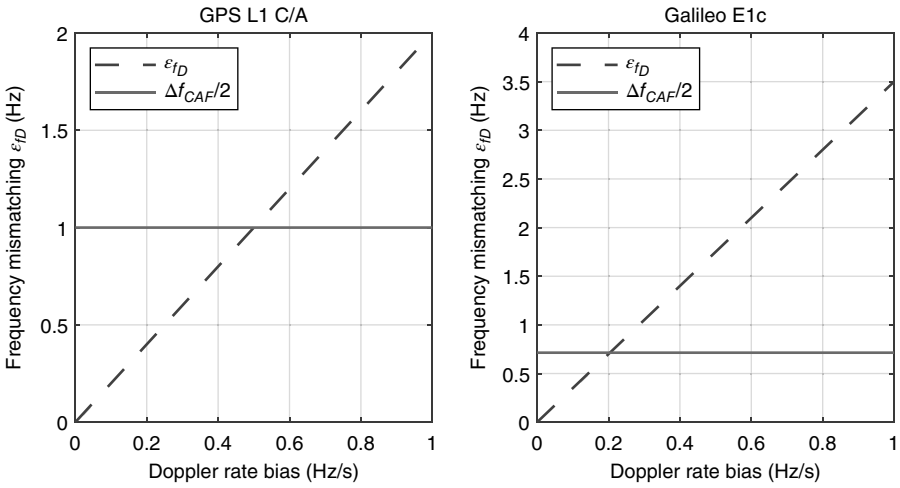

Figure 23.12 Theoretical Doppler rate error requirements for weak GNSS signal acquisition.

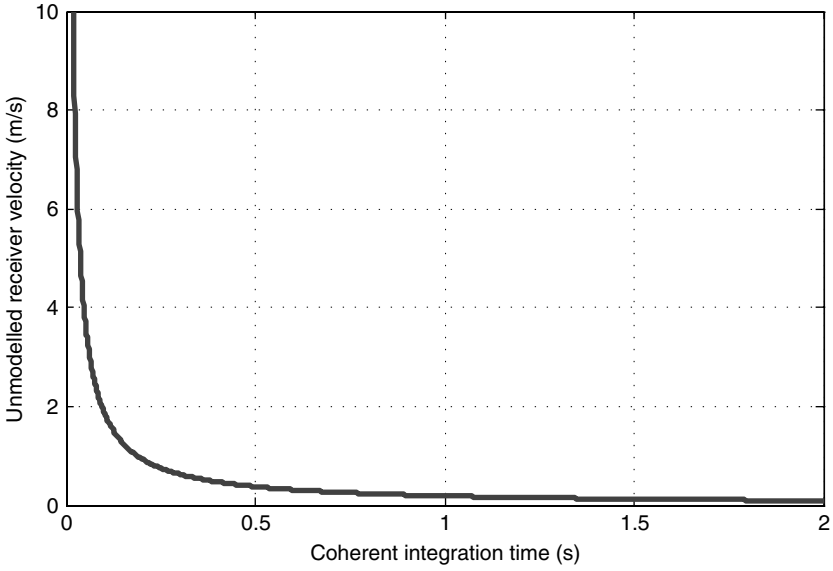

Figure 23.13 Maximum allowable unmodelled receiver velocity as a function of coherent integration time.

23.4.6 Other Factors Impacting Receiver Sensitivity

- **Interference.** RFI is caused by electronic equipment (such as television, mobile, and very high frequency [VHF] transmitters) radiating in the proximity of the GPS frequency band, or by intentional transmission of in-band RF signals (e.g., jamming and spoofing).
- **Multipath reflections.** Multipath causes additional power losses (fading) and measurement biases. In some cases, where the line-of-sight (LOS) signal is

completely obscured, the preudorange can be estimated by using non-LOS (NLOS) signals, which are inherently weaker.

- **Near–far effect.** Dealing with a mix of strong and weak signals at the same time is a challenging problem. This happens especially in indoor, urban, and space environments, where high-sensitivity techniques are employed. False locks can be generated by the autocorrelation of a PRN code with itself, or by the cross-correlation between different ranging codes. In such cases, the risk is to detect and track a peak from an unwanted and much stronger signal, rather than the correct peak of the desired weak signal.
- **Satellite visibility.** At least four satellites are required to produce a valid navigation solution. In all those situations in which some signals are received at a C/N_0 below the receiver sensitivity, the solution availability may be jeopardized. Multiconstellation provides more ranging signals and thus improves satellite geometries. This can be seen as an alternative way to improve the receiver sensitivity, as reported in Section 23.7.

23.5 HIGH-SENSITIVITY RECEIVER DESIGN

The design of GNSS receivers for high-sensitivity focuses mainly on the acquisition and tracking stages. The main challenge is the determination of the correlation peak and thus the estimation for the signal code phase. In particular, in the acquisition stage the risk is to fail in identifying the correct correlation peak. In the tracking stage, low C/N_0 leads to loss of tracking lock.

23.5.1 Acquisition Stage

Standard acquisition schemes are designed to work in open-sky conditions, where the antenna is expected to capture nominal received signal strength. In harsh environments, GNSS receivers have to deal with a reduced power level. Exploiting the direct-sequence spread spectrum (DSSS) nature of CDMA signals, a higher despreading gain can be achieved. This results in an SNR improvement in the CAF after the correlation process.

Therefore, the first strategy for increasing the acquisition sensitivity is the integration time extension. However, as briefly mentioned in Section 23.3.1, this is limited by several factors:

- the presence of unknown navigation data bit transitions, which imposes the condition $T_c \leq T_b$;
- the presence of a secondary code in pilot signals, which, although being a known sequence, still requires proper synchronization;
- the reduction of the acquisition Doppler bin size and thus the increase of the SS size and of the computational complexity.

Therefore, a trade-off between the sensitivity improvement and the complexity increase should be considered when changing the value of the integration

time. Most of these limitations can be mitigated with the noncoherent combination of short coherent integrations, as described in Section 23.3.2. However, this approach leads to lower processing gains and, therefore, a second trade-off is usually made between the coherent integration time and the number of noncoherent combinations.

In the acquisition stage, the presence of a bit transition acts as a sort of subcarrier, which splits the main lobe of the spectrum in two side peaks, symmetric with respect to the correct bin, leading to an incorrect acquired Doppler frequency. The shape of the two lobes and the relative amplitudes of the peaks depend on the position of the bit transition. An example of GPS SIS acquisition, characterized by a phase transition in the middle of the observation windows, is reported in Figure 23.19 and will be described later on.

Statistical Characterization of the Acquisition As remarked in Section 21.3.1, GNSS signal acquisition can be seen as a detection problem. Therefore, each value X of the search space, as defined in Equation 21.37, i.e., the correlation output for each for each bin of the SS, can be modeled as a random variable. The maximum of the SS (S_{max}, Eq. 21.31) is then used as a test statistic and compared against a threshold θ_t, to test two hypothesis:

- H_0, the null hypothesis, if only noise is present;
- H_1, the so-called alternative hypothesis, if the signal is present, along with noise, and is correctly aligned.

Recalling the expression of the CAF for coherent and noncoherent schemes, reported respectively in Sections 23.3.1 and 23.3.2, and assuming Gaussian noise, its theoretical distribution can be computed. Thus, the probability density function (PDF) of the random variable can be derived, both for coherent and noncoherent schemes. An exhaustive theoretical derivation can be found in Reference 8.

The expression of the CAF in the case of coherent integration was reported in Equation 23.12. $S_{y,r,c}(\overline{\tau}, \overline{f}_D)$ is the square absolute value of a complex Gaussian random variable, with independent real and imaginary parts $Y_I(\overline{\tau}, \overline{f}_D)$ and $Y_Q(\overline{\tau}, \overline{f}_D)$. Their variance can be computed as:

$$
\begin{aligned}
&\mathrm{Var}\left[Y_1(\overline{\tau}, \overline{f}_D)\right] \\
&= \mathrm{Var}\left[\Re\left\{\frac{1}{N_c L}\sum_{n=0}^{N_c L-1} y_{\mathrm{IF}}[n]\, c_b(nT_s - \overline{\tau}) e^{j2\pi(f_{\mathrm{IF}}+\overline{f}_D)nT_s}\right\}\right] \\
&= \mathrm{Var}\left[\frac{1}{N_c L}\sum_{n=0}^{N_c L-1} y_{\mathrm{IF}}[n]\, c_b(nT_s - \overline{\tau})\cos(2\pi(f_{\mathrm{IF}}+\overline{f}_D)nT_s)\right] \\
&= \frac{1}{N_c^2 L^2}\sum_{n=0}^{N_c L-1} \mathrm{Var}\left[y_{\mathrm{IF}}[n]\, c_b(nT_s - \overline{\tau})\cos(2\pi(f_{\mathrm{IF}}+\overline{f}_D)nT_s)\right] \\
&= \frac{1}{N_c^2 L^2}\sum_{n=0}^{N_c L-1} \frac{\sigma_{IF}^2}{2} = \frac{\sigma_{IF}^2}{2N_c L},
\end{aligned}
\tag{23.25}
$$

where σ_{IF}^2 is the noise variance of the digital IF SIS, as defined in Eq. 21.20. Similarly, it can be proven that $\mathrm{Var}[Y_Q(\overline{\tau},\overline{f}_D)] = \dfrac{\sigma_{IF}^2}{2N_cL}$, and thus the coherent noise variance is:

$$\mathrm{Var}\left[Y_I\left(\overline{\tau},\overline{f}_D\right)\right] = \mathrm{Var}\left[Y_Q\left(\overline{\tau},\overline{f}_D\right)\right] = \frac{\sigma_{IF}^2}{2N_cL} = \sigma_c^2. \tag{23.26}$$

It is easy to observe that the variance of the noise is inversely proportional to N_c, confirming the benefits of coherent acquisition schemes.

Under the null hypotesis, $S_{y,r,c}(\overline{\tau},\overline{f}_D)$ is zero mean. Thus, $S_{y,r,c}(\overline{\tau},\overline{f}_D) \mid H_0$ follows a central χ^2 distribution (or Rayleigh distribution), with PDF:

$$f_c(s \mid H_0) = \frac{s}{\sigma_c^2} e^{-\frac{s^2}{2\sigma_c^2}}. \tag{23.27}$$

Under the alternative hypotesis, $S_{y,r,c}(\overline{\tau},\overline{f}_D)$ is no longer zero mean. The sum of the square of two nonzero mean independent Gaussian random variables leads to a noncentral χ^2 distribution (or Rice distribution), with PDF

$$f_c(s \mid H_1) = \frac{s}{\sigma_c^2} e^{-\frac{s^2+A^2}{2\sigma_c^2}} I_0\left(\frac{sA}{\sigma_c^2}\right) u(s), \tag{23.28}$$

A being the root mean square signal amplitude, $I_0(\cdot)$ the modified Bessel function of the first kind and zero order, and $u(s)$ the unit step function.

Considering N_n noncoherent integrations, the CAF $S_{y,r,n}(\overline{\tau},\overline{f}_D)$, given in Equation 23.12, is the sum of N_n independent χ^2 random variables with 2 degrees of freedom. Thus, under the null hypotesis, $S_{y,r,n}(\overline{\tau},\overline{f}_D)$ is a central χ^2 random variable with $2N_n$ degrees of freedom, with PDF:

$$f_n(s \mid H_0) = \frac{1}{2\sigma_c^2}\frac{1}{\Gamma(N_n)}\left(\frac{s}{2\sigma_c^2}\right)^{N_n-1} e^{-\frac{s}{2\sigma_c^2}}, \qquad s \geq 0. \tag{23.29}$$

Under the alternative hypotesis, $S_{y,r,n}(\overline{\tau},\overline{f}_D)$ is a noncentral χ^2 random variable with $2N_n$ degrees of freedom, with PDF:

$$f_n(s \mid H_1) = \frac{1}{2\sigma_c^2}\left(\frac{s}{A}\right)^{\frac{N_n-1}{2}} e^{-\frac{s+A}{2\sigma_c^2}} I_{N_n-1}\left(\frac{\sqrt{sA}}{\sigma_c^2}\right), \qquad s \geq 0. \tag{23.30}$$

Detection and False Alarm Probabilities The acquisition scheme performance can then be evaluated by means of probabilities. For a specific value of θ_t, there are four possible outcomes [1]:

- **detection probability,** P_d, the probability of correctly detecting the signal:

$$P_d = P(S_{max} > \theta_t \mid H_1); \tag{23.31}$$

- **miss detection probability,** P_{md}, the probability of missing the detection of the signal in the case of presence of the signal:

$$P_{md} = P(S_{max} \leq \theta_t \mid H_1) = 1 - P_d; \tag{23.32}$$

- **false alarm probability,** P_{fa}, the probability of detecting a wrong signal, in the case in which the true signal is not present

$$P_{fa} = P(S_{max} > \theta_t \mid H_0); \tag{23.33}$$

- **correct dismissal probability,** P_{cd} , the probability of correctly not detecting a signal in the case where the true signal is not present

$$P_{cd} = P(S_{max} \leq \theta_t \mid H_0) = 1 - P_{fa}. \tag{23.34}$$

In Figure 23.14, the PDFs for the H_0 and H_1 conditions are drawn respectively in pink and in green. The same figure reports the threshold θ_t and the different probabilities defined above, corresponding to the shaded area. If $f(s \mid H_1)$ and $f(s \mid H_0)$ are respectively the PDFs in the two test hypothesis, then the single cell detection and false alarm probabilities are defined as

$$P_d = \int_{\theta_t}^{+\infty} f(s \mid H_1)\,\mathrm{d}s \tag{23.35}$$

and

$$P_{fa} = \int_{\theta_t}^{+\infty} f(s \mid H_0)\,\mathrm{d}s. \tag{23.36}$$

In the case of coherent correlation, by substituting Equations 23.27 and 23.28 into Equation 23.36 and 23.35, respectively and by exploiting properties of central and noncentral χ^2 random variables [8,18], the following false alarm and detection probabilities are obtained:

$$P_{fa,c}(\theta_t) = e^{-\frac{\theta_t^2}{2\sigma_c^2}}, \tag{23.37}$$

and

$$P_{d,c}(\theta_t) = Q_1\left(\sqrt{\frac{A}{\sigma_c^2}}, \sqrt{\frac{\theta_t}{\sigma_c^2}}\right), \tag{23.38}$$

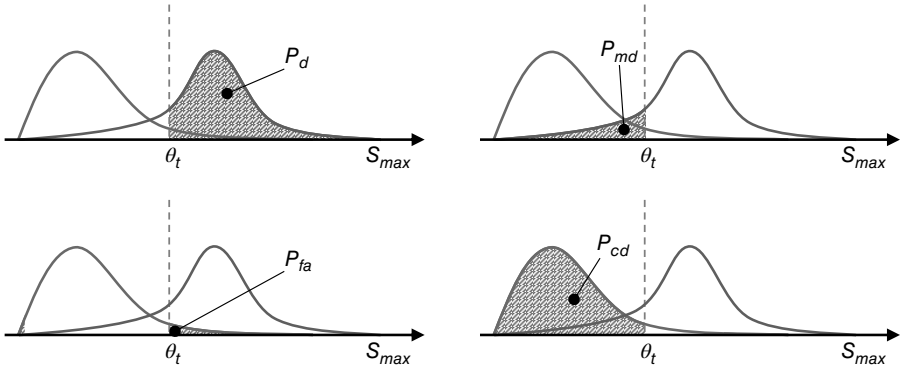

Figure 23.14 PDF in the case of H_0 and H_1 and related acquisition probability metrics.

where $Q_K(a,b)$ is the generalized Marcum Q-function, defined as:

$$Q_K(a,b) = \frac{1}{a^{K-1}} \int_b^{+\infty} x^K e^{-\frac{a^2+x^2}{2}} I_{K-1} ax \, \mathrm{d}x. \tag{23.39}$$

Similarly, in the case of noncoherent correlation, the following false alarm and detection probabilities are obtained:

$$P_{fa,n}(\theta_t) = e^{-\frac{\theta_t}{2\sigma_c^2}} \sum_{i=0}^{N_n-1} \frac{1}{i!} \left(\frac{\theta_t}{2\sigma_c^2} \right)^i, \tag{23.40}$$

and

$$P_{d,n}(\theta_t) = Q_K \left(\sqrt{\frac{KA}{\sigma_c^2}}, \sqrt{\frac{\theta_t}{\sigma_c^2}} \right). \tag{23.41}$$

The acquisition threshold is determined according to a required target P_{fa}, by using Equation 23.36, or to a maximum MAT. Therefore, for the case of coherent integration, the threshold corresponds to:

$$\theta_t = \sqrt{-2\sigma_c^2 \ln(P_{fa})}. \tag{23.42}$$

Once the acquisition threshold is set, the single cell detection probabilities can be evaluated, exploiting Equation 23.35.

It is straightforward to notice that higher coherent integration times (i.e., higher values of N_c) lead to lower values of σ_c^2, and in turn to lower false alarm probablities P_{fa} and to higher detection probabilities P_d, for a given threshold θ_t. The same considerations hold for N_n. From a graphical point of view, it can be shown that for higher values of N_c and N_n the probability distributions depicted in Figure 23.14 move away one from each other.

ROC Curves Once P_d and P_{fa} are obtained, they can be used to plot the receiver operating characteristic (ROC) curve, which depicts the trend of the false alarm probability versus the detection probability for different values of the threshold.

Figure 23.15 provides an example of a ROC curve for a GPS L1 C/A signal at 30 dB-Hz. The different points of the blue curve correspond to different values of θ_t. The curve highligths the fact that the lower the false alarm probability, the lower the detection probability.

The goal of a high-sensitivity receiver is indeed to move the working point in the area above the curve, so as to obtain low false alarm events and good detection probabilities at the same time. This can be achieved by exploiting coherent and noncoherent acquisition schemes. An example is provided in Figure 23.16, where it is shown that increasing the number N_c of coherent integrations, improves the performance, thanks to the reduction of the noise variance. When compared to noncoherent integration, coherent integration assures higher curves for the same total integration time.

Peak Separation Acquisition peak-to-floor ratio metrics have been proposed in Reference 12 to assess the performance of single acquisition trials. They are able to

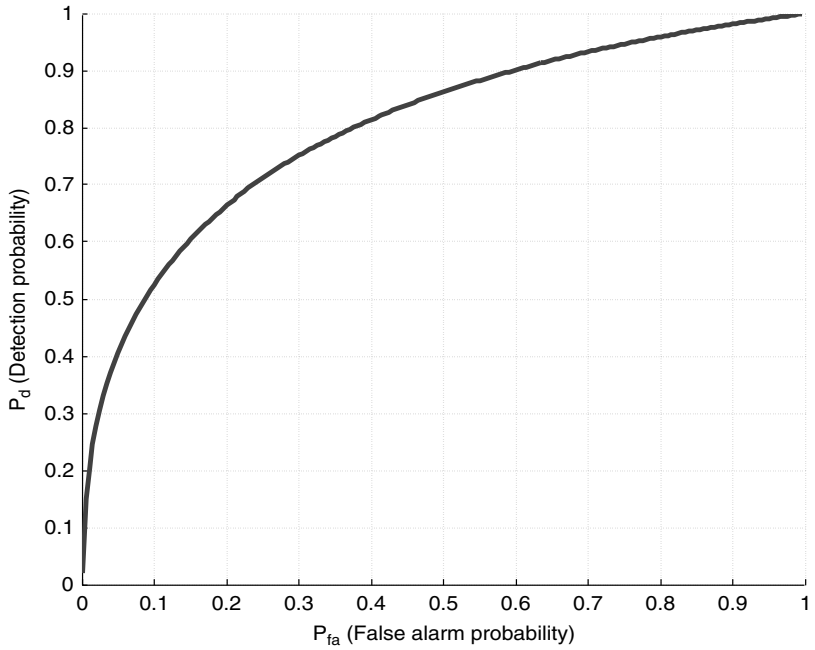

Figure 23.15 ROC curve for $C/N_0 = 30$ dB-Hz and for a single integration time period.

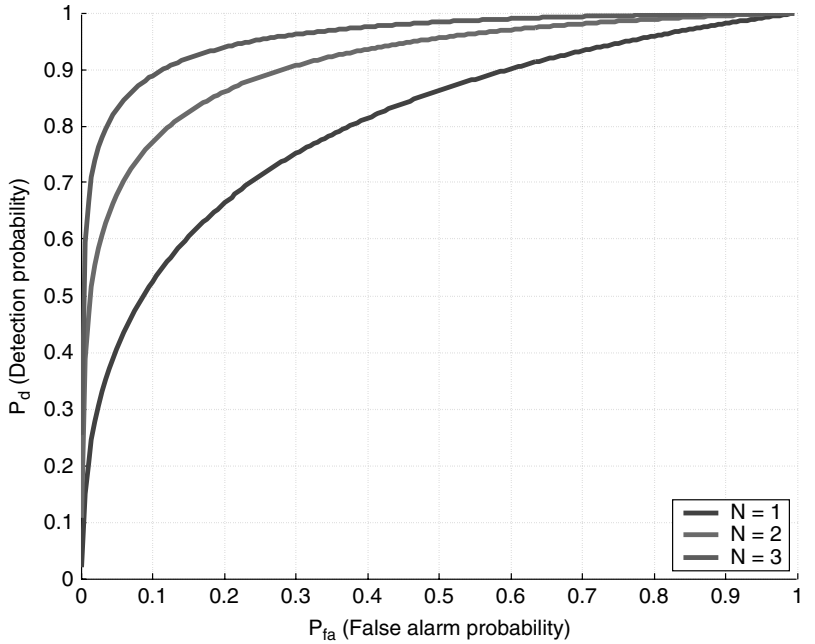

Figure 23.16 ROC curve for $C/N_0 = 30$ dB-Hz and different coherent integration values N_c.

highlight the overall postcorrelation SNR trend. In particular, two metrics can be defined, $\alpha_{\max}$ and α_{mean}:

$$\alpha_{\max} = \frac{|S_{max}|^2}{\max|S_{floor}|^2}, \tag{23.43}$$

$$\alpha_{\text{mean}} = \frac{|S_{max}|^2}{E\left[|S_{floor}|^2\right]}, \tag{23.44}$$

where S_{floor} stands for the floor values of the CAF, i.e., the values outside the signal correlation peak. Note that the shape of the correlation function may affect more than 1 bin of the SS depending on the sampling frequency. This is always true for the BOC signals. In case of low noise, the peak separation metrics mainly depend on the correlation properties of the spreading codes.

Examples of Coherent and Noncoherent Accumulations This section reports some examples of acquisition results, underlying the advantages of performing coherent and noncoherent acquisition. Results are obtained processing a GPS L1 C/A legacy signal generated by a software GNSS signal simulator [19] through a fully software GNSS receiver.

GPS L1 C/A signal at nominal C/N_0 First, a signal characterized by C/N_0 around the nominal value is considered, to analyze the impact of larger integration times in the CAF evaluation. A GPS L1 C/A signal at 45 dB-Hz is processed. The code delay is equal to 512 chips, while the Doppler frequency amounts to 1500 Hz + 0.1 Hz/s.

Figure 23.17 reports the acquisition results, obtained running the software receiver with a standard configuration. The coherent integration time is $T_c = 1$ ms and no noncoherent accumulations are performed ($N_n = 1$). The total frequency search space is set to 10.125 kHz. The width of the frequency bin Δf is set according to Equation 23.33, and equal to 667 Hz; therefore, the total number of frequency bins is $N_{\text{bin}} = 15$. The left part of the figure reports the three-dimensional CAF, while on the right the monodimensional code delay domain and frequency delay domain correlations are reported. As expected, the receiver can successfully acquire the signal; the peak clearly emerges from the noise floor and the parameters $\hat{f}_D$ and $\hat{\tau}$ can be correctly estimated. The acquisition metrics, evaluated running 1000 Monte Carlo simulations, are $\alpha_{max} = 5.3$ and $\alpha_{mean} = 912$.

When doubling the coherent integration time, $T_c = 2$ ms, the correlation peak amplitude increases, as does the postcorrelation SNR, at the expenses of a larger MAT or computational burden. Δf is now equal to 333 Hz, and the total number of frequency bins is $N_{\text{bin}} = 30$. The acquisition result is reported in Figure 23.18. The width of the sinc in the frequency domain plot halved, while the correlation peak emerges even more clearly than in the previous example. The acquisition metrics, evaluated running 1000 Monte Carlo simulations, are $\alpha_{max} = 16.5$ and $\alpha_{mean} = 2398$.

It is possible to extend the integration time up to the instant in which the first bit transition happens. In this specific case, when increasing T_c to 20 ms, a bit transition induces a failure in the acquisition process. As detailed in Section 23.5.1, the correlation peak is doubled because of the subcarrier effect of the phase reversal. In

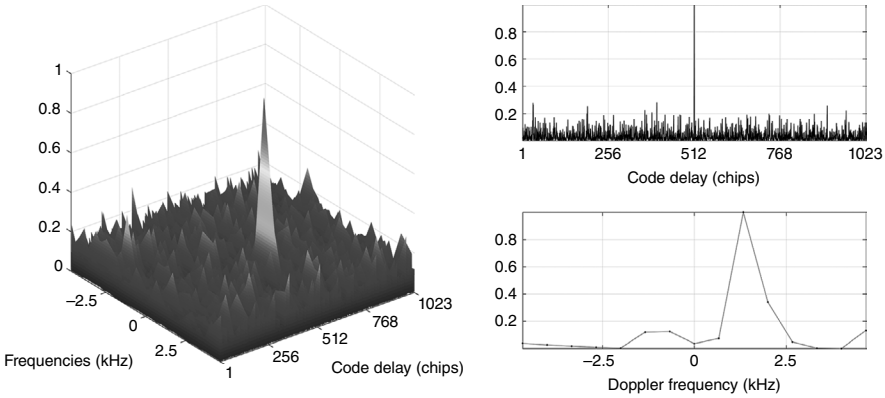

Figure 23.17 Acquisition results for a GPS L1 C/A signal at 45 dB-Hz, with $T_c = 1$ ms and $N_n = 1$.

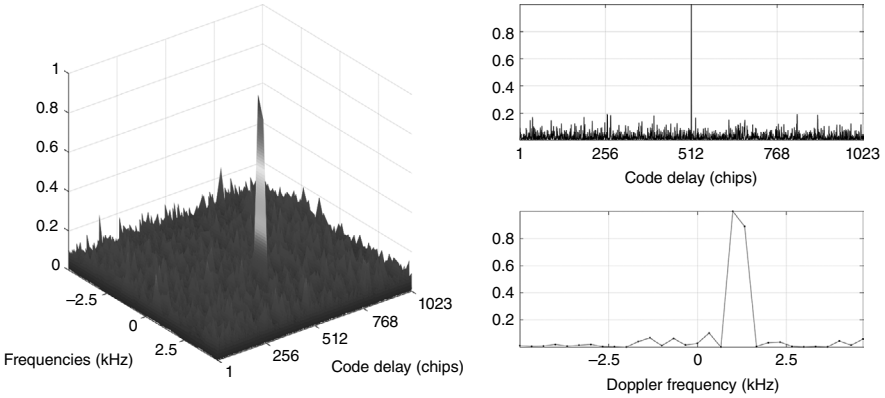

Figure 23.18 Acquisition results for a GPS L1 C/A signal at 45 dB-Hz, with $T_c = 2$ ms and $N_n = 1$.

this case it is not possible to correctly estimate code delay and Doppler frequency. Acquisition results for this case are reported in Figure 23.19 (the three-dimensional plot is enlarged to better identify the correlation peak).

If, rather than 20 coherent summations, 20 noncoherent summations are performed, the bit transition problem is avoided and the peak is correctly identified, as reported in Figure 23.20. Being $T_c = 1$ ms, the width of the sinc function is equal to the case reported in Figure 23.17.

GPS L1 C/A Signal at C/N_0 below the Nominal Value When moving to signals characterized by a lower C/N_0 it is harder to acquire them using a standard scheme. In this example, a signal at $C/N_0 = 35$ dB-Hz is considered. A standard acquisition scheme with $T_c = 1$ ms and $N_n = 1$ fails in acquiring the signal, as reported in Figure 23.21.

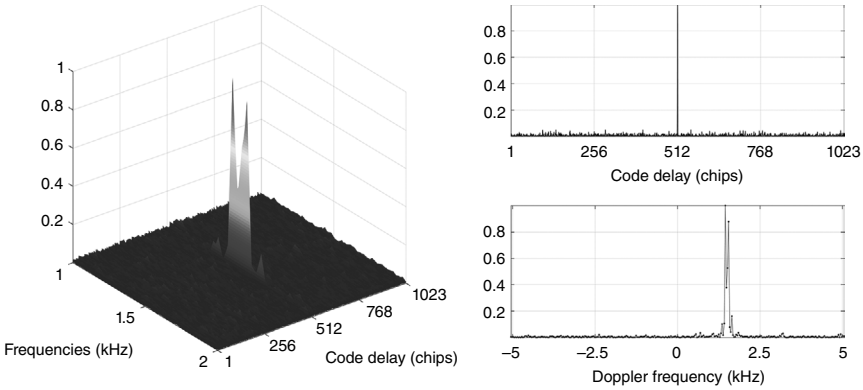

Figure 23.19 Acquisition results for a GPS L1 C/A signal at 45 dB-Hz, with $T_c = 20$ ms and $N_n = 1$.

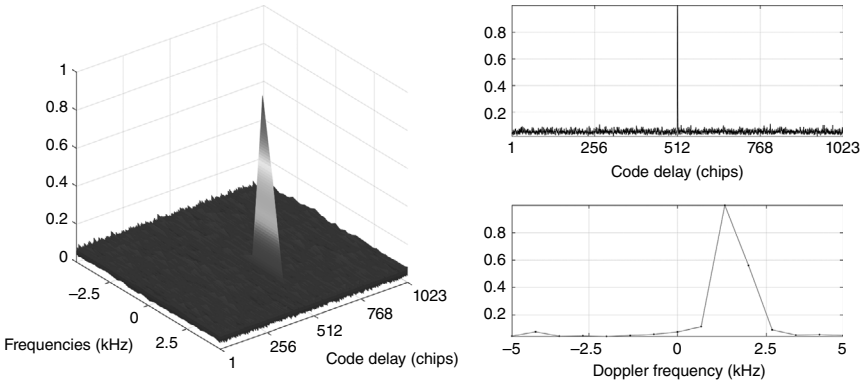

Figure 23.20 Acquisition results for a GPS L1 C/A signal at 45 dB-Hz, with $T_c = 1$ ms and $N_n = 20$.

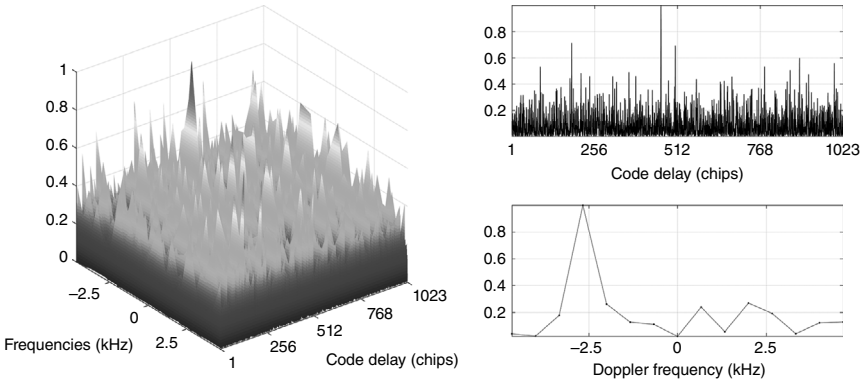

Figure 23.21 Acquisition results for a GPS L1 C/A signal at 35 dB-Hz, with $T_c = 1$ ms and $N_n = 1$.

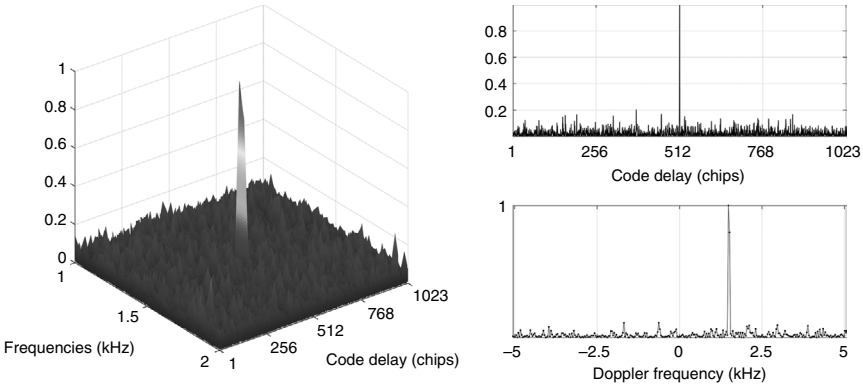

Figure 23.22 Acquisition results for a GPS L1 C/A signal at 35 dB-Hz, with $T_c = 20$ ms and $N_n = 1$.

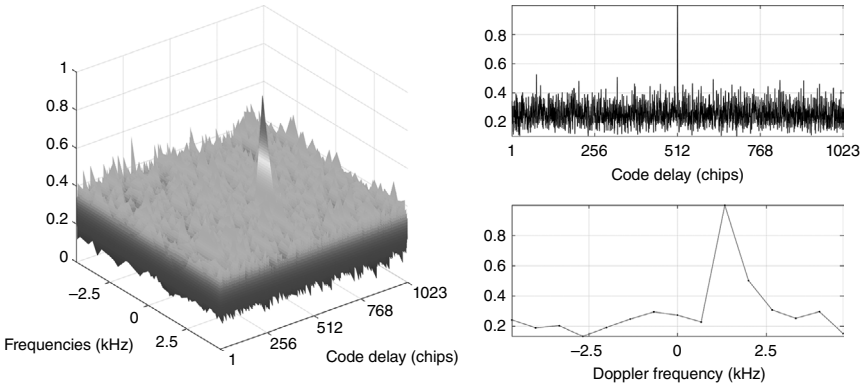

Figure 23.23 Acquisition results for a GPS L1 C/A signal at 35 dB-Hz, with $T_c = 1$ ms and $N_n = 20$.

When increasing the coherent integration time T_c to 20 ms, and assuming a correct bit synchronization, the signal is correctly acquired, as shown in Figure 23.22. In this case $\alpha_{max} = 13.5$ and $\alpha_{mean} = 2459$.

Alternatively, it is possible to acquire the signal by performing noncoherent integrations. For example, with settings $T_c = 1$ ms and $N_n = 20$, the total observation time is equal to 20 ms, as in the previous case. However, the noncoherent gain is lower, resulting in lower acquisition metrics, $\alpha_{max} = 3.2$ and $\alpha_{mean} = 15.6$. Also from visual inspection of the acquisition results, reported in Figure 23.23, it is clear that the postcorrelation SNR is lower, although it is being correctly detected.

A further step can be done, moving to signals characterized by a lower C/N_0, around 30 dBHz. In this case it is still possible to acquire the signal by fixing the coherent integration time to 20 ms and performing $N_n = 20$ noncoherent summations, thus spanning a total integration time of 400 ms. The acquisition results are reported in Figure 23.24. Also in this case the CAF plot is enlarged in the frequency range.

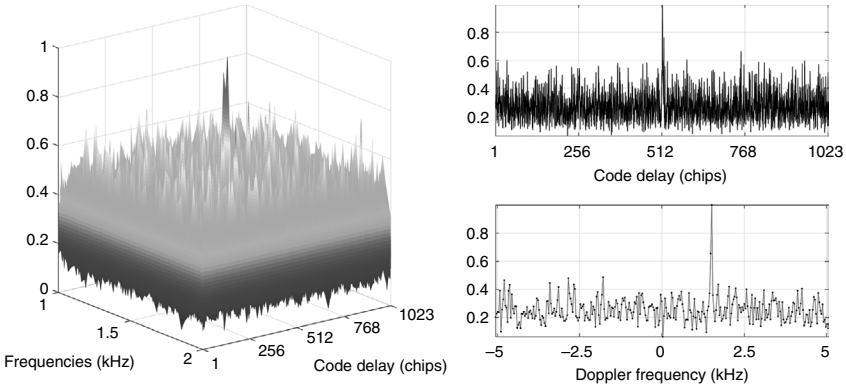

Figure 23.24 Acquisition results for a GPS L1 C/A signal at 30 dB-Hz, with $T_c = 20$ ms and $N_n = 10$.

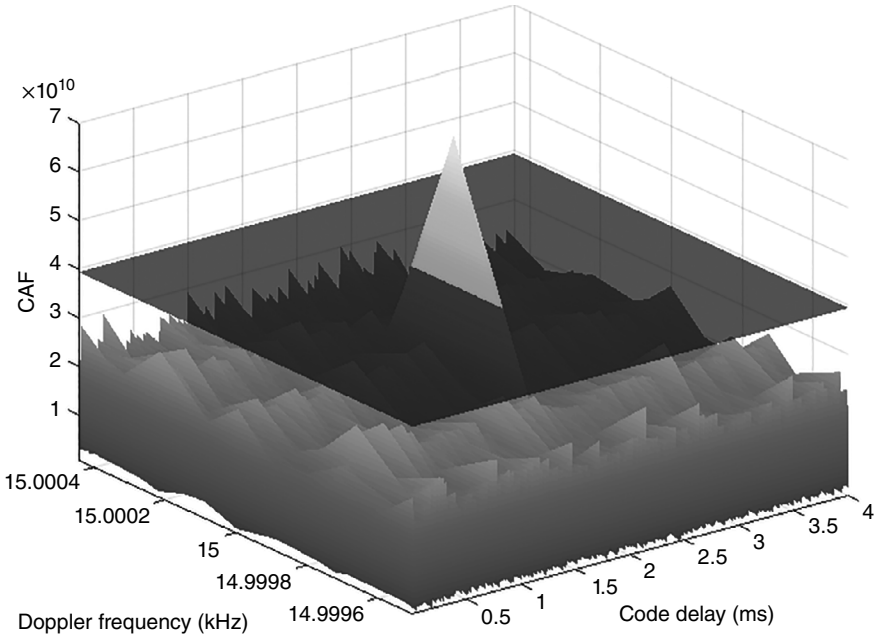

Figure 23.25 Acquisition results for a Galileo E1c at 5 dB-Hz, with $T_c = 3$ s and $N_n = 8$.

Galileo E1c Signal at Very Low C/N_0 When dealing with very weak signals, it is suitable to exploit dataless pilot components of new and modernized GNSS, such as Galileo E1c. When dealing with very low C/N_0, around 5 and 10 dB-Hz, it is necessary to considerably extend the coherent integration time and the number of noncoherent sums. As described in Section 23.4, some further compensations regarding Doppler, Doppler rate, and clock stability have to be taken into account.

Figure 23.25 reports the acquisition results of a Galileo E1c signal at 5 dB-Hz. The coherent integration time has been extended to $T_c = 3$ s, while $N_n = 8$ noncoherent

TABLE 23.2. Coherent Integration Time and Noncoherent Accumulations for Very Weak GNSS Signals Acquisition

Signal	5 dB-Hz	10 dB-Hz
GPS L1 C/A	$T_c = 2$ s; $N_n = 6$	$T_c = 0.5$ s; $N_n = 8$
Galileo E1c	$T_c = 3$ s; $N_n = 8$	$T_c = 0.7$ s; $N_n = 10$

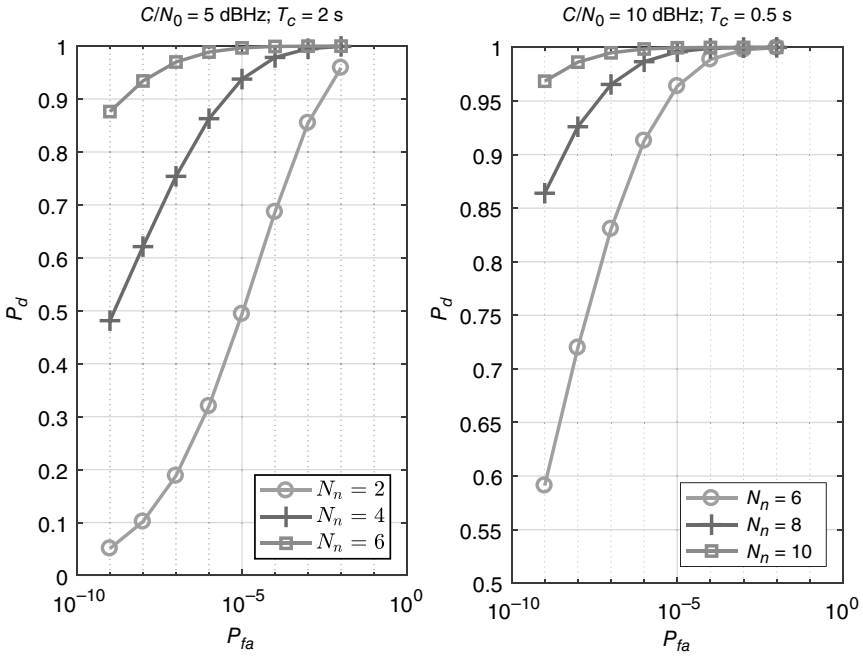

Figure 23.26 ROC curve for very weak GPS L1 C/A signals.

sums were considered, thus spanning a total integration time equal to 24 seconds. The Doppler frequency range has been considerably reduced to achieve a reasonable MAT. The correlation peak clearly emerges from the noise floor, both in the frequency and in the code delay domains.

Table 23.2 provides a summary of the minimum coherent integration time T_c and noncoherent accumulations N_n allowing acquisition of a very weak GNSS signal, with detection probability $P_d = 90\%$ for a given false alarm probability $P_{fa} = 10^{-8}$.

Figure 23.26 provides the ROC curve for GPS L1 C/A code acquisition at very low C/N_0 (5 dB-Hz in the left plot, 10 dB-Hz in the right plot). The curves prove that, in order to achieve correct detection of the main correlation peak with high probability, extension of the coherent integration time up to 2 s and 0.5 s is needed for acquisition at 5 and 10 dB-Hz, respectively. In addition, a proper number of noncoherent accumulations is needed in order to achieve a detection

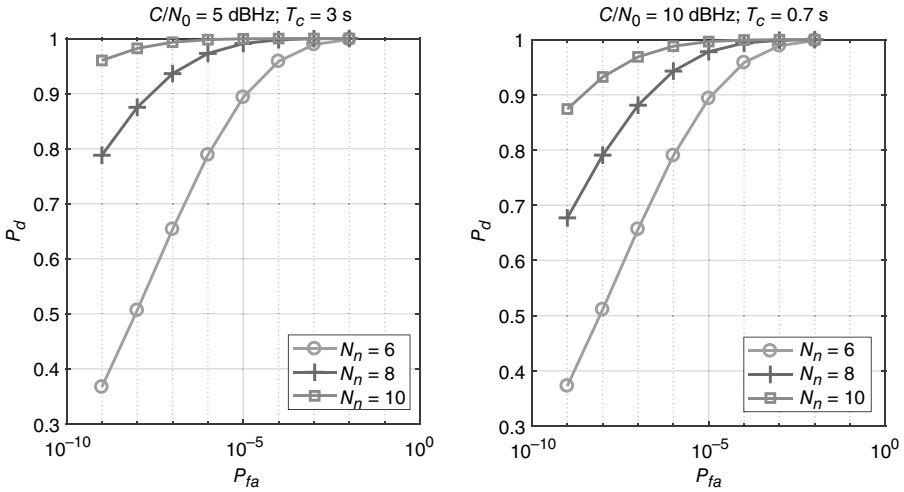

Figure 23.27 ROC curve for very weak Galileo E1c signals.

probability over 90% even at very low false alarm probability (very high detection threshold).

AU: Could you expand this acronym and have the acronym then in parentheses behind the expansion?

Figure 23.27 provides the ROC curve for the Galileo E1c channel acquisition at 5 dB-Hz (left plot) and 10 dB-Hz (right plot). The full CBOC modulation has been considered, thus assuming $f_s = 50$ MHz and $B_{IF} = 20.46$ MHz. A larger coherent integration time with respect the case of GPS L1 acquisition has to employed, due to the increased front-end filter bandwidth which makes more noise power going through the correlator. A coherent integration time up to 3 and 0.7 s has to be employed for the full CBOC acquisition down to 5 and 10 dB-Hz, respectively. It has to be mentioned that such ROC curves do not take into account possible losses due to the front-end filtering, quantization, and/or frequency mismatching, the details of which can be found in Reference 4.

Acquisition in the Presence of High Doppler Rate The theoretical requirements on the Doppler rate aiding error reported in Figure 23.12 have been confirmed in Reference 14 by a set of simulations exploiting a fully software GNSS receiver. A fully software GNSS signal generator [19] has been adopted for generating a GPS L1 C/A and a Galileo E1c signal at 10 dB-Hz, affected by Doppler frequency equal to 15 kHz and by a code delay equal to half of the primary code period (0.5 ms and 2 ms, respectively).

Figure 23.28 shows the GPS L1 acquisition performance at 10 dB-Hz for different values of the bias between the Doppler rate aiding and the true Doppler rate affecting the simulated signals. The two plots on top show the acquisition metrics α_{mean} and α_{max}. The two plots on bottom show the code delay and Doppler frequency estimated by the aided acquisition process. It can be observed that correct acquisition of the code delay is achieved for Doppler rate bias values up to 0.44 Hz/s. However, it can be observed also that, increasing the Doppler rate bias, a loss on the correlation amplitude is detected due to the increasing frequency mismatching error.

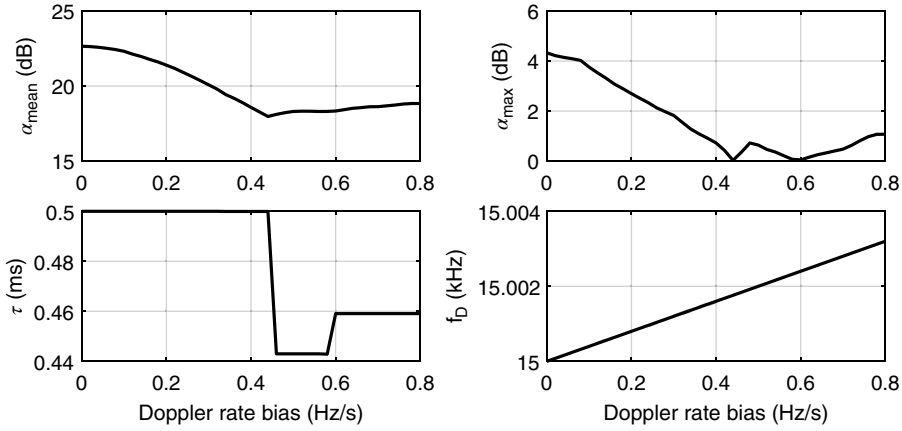

Figure 23.28 GPS L1 C/A code acquisition performance with respect the Doppler rate bias.

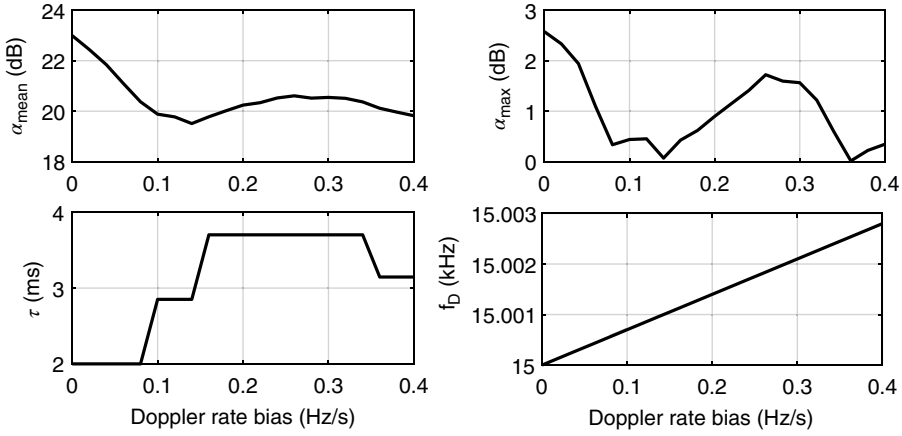

Figure 23.29 Galileo E1c code acquisition performance with respect the Doppler rate bias.

Figure 23.29 shows the Galileo E1c acquisition performance at 10 dB-Hz for different values of the Doppler rate bias. In this case, correct acquisition is achieved up to a Doppler rate error equal to 0.08 Hz/s, as confirmed by the correct estimation of the code delay.

As expected, the acquisition performance reported in Figures 23.28 and 23.29 is slightly worse with respect to the theoretical results reported in Figure 23.12 due to the presence of additional factors like noise, cross-correlation with other received PRNs, and quantization losses.

23.5.2 Transition between Acquisition and Tracking

Propagation of the Doppler frequency estimate from the acquisition to the tracking block has to be carefully designed. This is particularly important in those harsh GNSS environments characterized by weak GNSS signals and high dynamic. Integration of acquisition and tracking blocks with a receiver-based Doppler aiding system is a sensitive process, since accurate Doppler rate estimation has to be propagated at the tracking level to help the local oscillator. However, especially for long integration periods, an extremely stable receiver clock is required even in presence of an accurate Doppler aiding system.

23.5.3 Tracking Stage

Tracking loops have been described in Chapter 21. A tracking loop consists of an integrator, a discriminator, a loop filter, and a numerical controlled oscillator (NCO), and is able to provide, at each iteration, an estimate of the quantity to be tracked. In the case of GNSS, tracking loops are used to track the frequency, phase, and code delay of the incoming signal in order to perform carrier wipe-off and code wipe-off and to compute the pseudoranges. Frequency lock loops (FLLs), phase lock loops (PLLs), and delay lock loops (DLLs) are used in a concatenated scheme.

In standard receivers, the integration period is set equal to the bit duration (1 ms for GPS C/A signals). However, in harsh environments, it is necessary to increase the integration time to reduce the impact of noise. Particular attention is given in the literature to techniques for coherently increasing the integration time in the tracking stage [20]. Once the bit synchronization is achieved, it is possible to increase the integration time up to the navigation message bit duration T_b, 20 ms for GPS L1 C/A.

However, as briefly mentioned in Section 23.3.1, this is limited by several factors:

- the presence of unknown navigation data bit transitions, which imposes the condition $T_c \leq T_b$;
- the presence of a secondary code in pilot signals, which, although being a known sequence, still requires proper synchronization;
- the reduction of the acquisition Doppler bin size and thus the increase of the SS size and of the computational complexity;
- the instability of tracking loop filters that are usually designed for low integration times and relatively large loop bandwidths;
- the loss of coherency, introduced by the varying Doppler frequency, the clock instability, the varying code rate, and the receiver dynamics throughout the coherent integration period.

The sensitivity of a tracking loop can be evaluated measuring the *tracking jitter*. The tracking jitter is a measure of the amount of noise transferred from the input signal to the output of the loop on the final paramter estimate. It is the first

measure of a loop performance and allows one to quantify the impact of the thermal noise. It is defined as:

$$\sigma_j = \frac{\sigma_r}{G_d}\sqrt{2B_nT_c}\,, \tag{23.45}$$

where

- σ_r is the standard deviation of the noise at the output of the discriminator;
- B_n is the equivalent bandwidth of the loop;
- G_d is the discriminator gain.

The tracking jitter is a normalized version of the noise standard deviation, taking into account the bandwidth of the complete loop. The theoretical expression of the tracking jitter in a standard PLL is:

$$\sigma_j = \sqrt{\frac{B_n}{C/N_0}\left(1+\frac{1}{2C/N_0\,T_c}\right)}. \tag{23.46}$$

Figure 23.30 shows the tracking jitter for different C/N_0 values, summarizing the performance of a PLL/DLL tracking stage. The experimental tracking jitter is estimated according to Equation 23.45, performing Monte Carlo simulations, exploiting a software-based tracking stage and using signals generated by a software GNSS signal generator [19]. GPS L1 C/A signals are considered, characterized by a Doppler rate equal to about 1 Hz/s. The coherent integration time is set equal to $T_c = 20$ ms, while the loop bandwidth of the PLL and of the DLL is equal to 10 Hz and 2 Hz, respectively. The vertical line that corresponds to $C/N_0 = 33$ dB-Hz marks the point in which the loop is no longer in lock conditions. This means that the tracking sensitivity is equal to 34 dB-Hz. To track signals at a lower C/N_0 it is necessary to further extend the integration time.

In order to go beyond the limit imposed by the bit transitions, a solution is given by bit estimation and recovery techniques. On one hand, it is possible to foresee the value of the next navigation bit. On the other hand, any possible

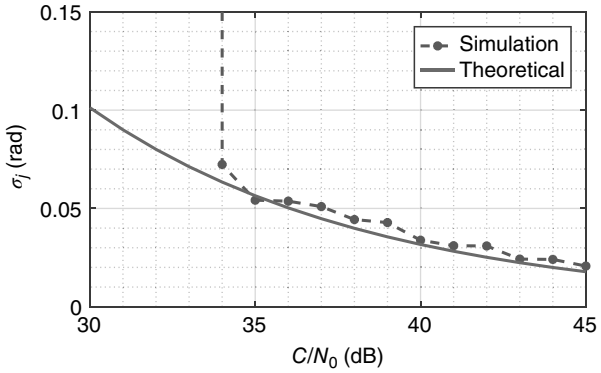

Figure 23.30 Tracking jitter for $T_c = 20$ ms and $N_n = 1$.

combination of the navigation message bits over the whole integration period can be tested and compared. The coherent integration time can indeed be extended, at the expense of a higher computational load, growing exponentially with the integration time. In addition, the bit estimation becomes unreliable at low C/N_0. This problem can be overtaken if assistance data are available. In this case, a perfect data wipe-off can be performed, as described in Section 23.4.1.

An alternative solution is to use discriminators insensitive to bit transitions, based on nonlinear operations, allowing, in principle, to extend arbitrarily the integration time. In Reference 21, a noncoherent architecture for GNSS tracking loops is proposed and analyzed, deriving a noncoherent phase discriminator from the maximum likelihood (ML) principle. The ML phase estimator in the presence of sign transitions is derived, under the assumption of data bits randomly distributed. Under this hypothesis, the navigation message bits can be removed by squaring the signal.

Figure 23.31 reports the comparison between theoretical and experimental tracking jitter obtained using a tracking structure employing the discriminator described in References 21 and 22. $N_n = 4$ noncoherent sums are considered. T_c is equal to 20 ms as in the previous example, and therefore, the global noncoherent integration time is equal to 80 ms. The PLL bandwidth has been reduced to 2.5 Hz in order to keep the product $B_n N_n T_c$ constant and equal to 0.2, and to maintain the loop filters stable. The input GNSS signals are the same as above. From the figure it is possible to see that the noncoherent gain pushes the tracking sensitivity down to 27 dB-Hz.

The main drawbacks of larger integration times in the tracking stage are summarized in the following:

- the need to compensate for the Doppler change within the integration period: Indeed, when the observation time increases, the Doppler rate effect on the code is no longer negligible and has to be corrected. If assistance information is available, a more accurate frequency wipe-off can be performed. Noncoherent schemes are more robust to frequency residual errors than coherent architectures.

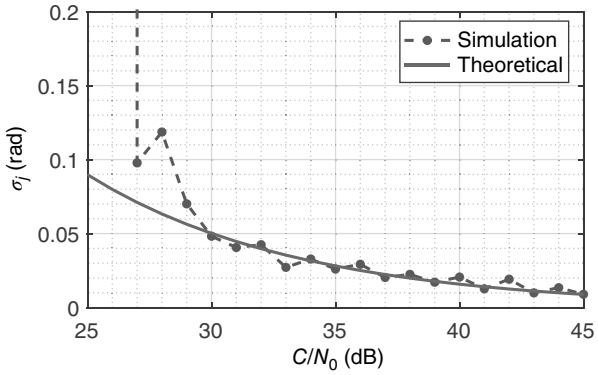

Figure 23.31 Tracking jitter for $T_c = 20$ ms and $N_n = 4$.

- the need to design proper discriminators, such as the ones described in References 21 and 22;
- The loop filters stability: Loop filters are designed to be stable for short coherent integration times. Alternative loop filters formulations have to be adopted, such as the controlled root formulation proposed in References 23 and 24.

23.6 HIGH SENSITIVITY AND A-GNSS

The topic of high sensitivity and harsh environment positioning is often linked to the argument of assisted GPS and GNSS. A-GNSS has been indeed designed not only to reduce the TTFF but also to increase the receiver sensitivity. Moreover, the two objectives are linked: the same aiding used to reduce the acquisition time can actually be exploited to improve the acquisition sensitivity. Most of the problems related to high-sensitivity acquisition and tracking presented above can be solved or eased exploiting proper external aiding. GNSS receivers, sensitivity can be enhanced if some a priori estimates of observables such as frequency offset, accurate time, code delay, and receiver position are known [4].

The core idea of A-GNSS is to assist the receiver providing all the information it would normally have obtained by processing the SIS through an alternative communication channel. The receiver keeps receiving and processing satellites signals, but thanks to assistance information it can do it faster and easier. Such aiding includes, but is not limited to:

- constellation almanac, to determine a priori the list of satellites in view and their approximate azimuth and elevation;
- precise ephemeris, to calculate the position of the satellites;
- receiver position estimate;
- approximate date and time (GPS time);
- ionospheric correction;
- accurate frequency reference to calibrate the local oscillator;
- satellite clock corrections;
- acquisition parameters (estimated Doppler shift, estimated delay).

For example, expected signal Doppler and Doppler rates can be used to reduce the frequency acquisition SS, and thus to make the acquisition process more robust to high dynamics, when large coherent integration times are employed. Similarly, some assistance servers are able to provide the content of the navigation message, which can be used to remove the data bits from the received signals, thus allowing extension of the coherent integration time beyond the data bit duration.

23.6.1 Example of Frequency Aiding in Acquisition

The availability of a rough estimates of the Doppler frequency is an added value for high-sensitivity receivers. In Section 23.4.3 it has been shown that for very

large integration times, required to acquire very weak signals, the acquisition time becomes extremely high, often unaffordable. As T_c increases, the number of frqeuency bins to be evaluated increases. A-GNSS gives a solutions to this: by reducing the total frequency SS, the number of bins can be reduced, and in turn, the MAT can be dramatically reduced. If the receiver is provided with a Doppler aiding accurate up to ϵ_{f_D}, the value of N_{bin} in the Doppler domain search can be reduced as follows:

$$N_{\text{bin}} = \left\lceil \frac{2\epsilon_{f_D}}{\Delta f} \right\rceil + 1. \tag{23.47}$$

Recalling the example reported in Section 23.4.3, a coherent acquisition time of 3 s leads to a total number of frequency bins $N_{\text{bin}} \simeq 44{,}000$. If frequency assistance is provided with an accuracy $\epsilon_{f_D} = \pm 50$ Hz, the frequency range in the SS is reduced. The number of bins decreases to about 450, as does the MAT.

In parallel, it has to be said that a small frequency SS also improves the acquisition performance. In Reference 15, the authors introduce a set of probability metrics at the SS level: the false alarm probability P_{FA} and the detection probability P_D. The P_{FA} at the SS level depends on the P_{fa} at cell level, defined in Equation 23.33, according to the following equation:

$$P_{FA} = 1 - \left[1 - P_{fa}(\theta_t)\right]^N, \tag{23.48}$$

θ_t being the acquisition threshold and N the total number of cells in the SS. According to Equation 23.48, fixing a required false alarm at cell level P_{fa}, a reduction of the SS size allows the achievement of better P_{FA} values.

As an example, Figure 23.32 shows the trend of the P_{FA} at the SS level with respect the P_{fa} at cell level for different values of the Doppler aiding accuracy ϵ_{f_D}. Fixing $P_{fa} = 10^{-8}$, a Doppler aiding accurate up to 1.5 Hz is needed to achieve a $P_{FA} = 10^{-2}$, in the case of Galileo E1c acquisition at 10 dB-Hz, exploiting $T_{\text{int}} = 0.7$ s combined with $N_n = 10$ noncoherent accumulations.

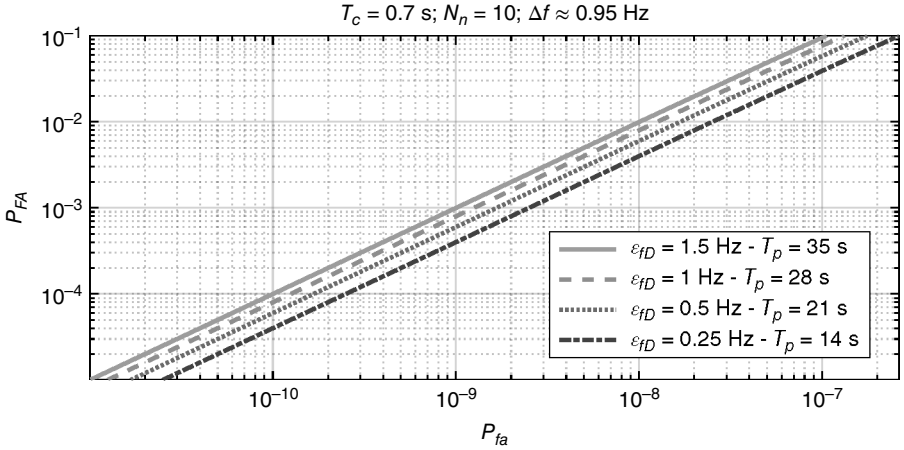

Figure 23.32 Galileo E1c noncoherent acquisition: acquisition metrics P_{FA} vs P_{fa} for different aiding scenarios.

23.7 NEW AND MODERNIZED GNSS

New and modernized GNSS signals offer users great opportunities for increasing the availability and accuracy of the positioning solutions. On one side, GPS and GLONASS are undergoing a modernization process. On the other side, new constellations, such as Galileo, Beidou, and the regional Indian and Japanese systems are by now operational. A complete description of the new signals is provided in Chapter 20. Throughout this chapter, only the GPS L1 C/A legacy signal has been considered. This section briefly outlines the main advantages of GPS and Galileo new civil signals from the perspective of high sensitivity.

23.7.1 Longer Code Periods

In Section 23.2.1 the impact of the code length in the correlation process has been evaluated. In particular, Example 23.1, showed how a longer spreading code can improve the correlation performance. This is the main reason why some of the new signals employ longer codes. For instance, Galileo E1b signals are modulated by 4 ms long memory codes. Other signals, such as GPS L2C, feature a more complex code structure, with a *moderate* and a *long* code multiplexed. While the moderate code is 20 ms long, the long code lasts for 1500 ms. GPS L5 signals, both in the in-phase and in the quadrature component, and Galileo E5a-I and E5a-Q signals, use 1-ms-long codes. However, they are transmitted at a higher code rate, 10.23 MHz.

A higher despreading gain can therefore be obtained, at the expense of a higher complexity and computational burden. It is also important to recall that signals characterized by a larger code rate require a larger front-end bandwidth, allowing more noise to enter the acquisition and tracking stages.

23.7.2 Pilot Channels

The main advantage of new and modernized signals for what concerns high-sensitivity capabilities is the presence of dataless signals, called *pilot* signals. Pilot signals are not modulated by the navigation message and can be used to assist the acquisition of and tracking of data signals. The absence of the navigation data bits allows the extension of the coherent integration time, avoiding any problem related to bit transitions. Dataless signals are broadcast by GPS (L1C, L5Q) and by Galileo (E1c, E5a-Q, E5b-Q, E6).

In addition, pilot signals are modulated by a secondary code. In order to extend the coherent integration time, synchronization with the secondary code has to be achieved, as detailed in Section 23.4.2.

23.7.3 Encoded Naviagtion Data

Modernized GNSS signals also feature encoded navigation data. As an example, GPS L2C navigation bits are encoded with a continuous FEC at a rate of 1/2. This allows to reach lower BERs at a lower C/N_0, improving the performance in harsh environments.

23.7.4 Different SS Definition

The definition of the number of bins of the SS to be evaluated during the acquisition phase changes for each signal. As described in Equation 23.20, the maximum Doppler frequency depends on the maximum satellite velocity, which in turn depends on the constellation orbits. The radius of the satellite orbit is equal to 26,560 km for GPS and to 29,600 km for Galileo. Therefore, the maximum Doppler shift experienced by Galileo signals is slightly lower, around 4.2 kHz. However, as the code period of Galileo satellites is higher (e.g., 4 ms for Galileo E1b), the bin size is about four times smaller. Therefore, even though the total Doppler range to be evaluated is lower, more bins are required, thus increasing the MAT.

23.8 CONCLUSIONS

In this chapter some of the basic concepts of signal processing for high-sensitivity GNSS receivers were given. To counteract for the low C/N_0 of the GNSS signals in harsh environments, particular strategies and techniques shall be considered. First, a recall on the signal power, signal noise and correlation gain has been provided. Then, the concept of integration time extension has been outlined by describing coherent and noncoherent solutions and by providing examples and by proposing solutions to the main issues revealed. A focus on the acquisition and tracking stages of a high-sensitivity receiver was then provided, along with an overview on assistance techniques and on new and modernized GNSS signals. The examples and the case studies presented show how high-sensitivity receivers are able to acquire and to track signals even at very low C/N_0, allowing the computation of a PVT solution in environments in which standard receivers would fail.

APPENDIX A

MATLAB Code

A.1 Example 1: Extension of the Code Length

The MATLAB code reported below has been used to generate the figures in Example 23.1.

```
% --- Clean up the environment
clear
close all
clc

% --- Variables definition
Rc = 0.5e6;          % Code Rate (chip /s)
Fs = 8e6;            % Sampling Frequency (Hz)

% --- define PRN codes
cLoc1 = [1 -1 1 -1 -1 -1 -1 1 -1 ...
         1 -1 -1 -1 1 -1 -1 1 1 1 -1];
```

```
cLoc2 = [ 1 1 -1 1 -1 1 1 -1 -1 1 ...
          1 1 1 1 -1 -1 -1 1 1 -1 1 ...
          1 1 -1 1 -1 1 -1 -1 -1 -1 ];

% cLoc = cLoc1;
cLoc = cLoc2;

L = length (cLoc); % Code Length (chip)
N = floor (Fs*L/Rc);      % Code Length (samples)

% --- Sample the local code
k = 0:N-1;
cLocSampled = cLoc (floor (k*Rc/Fs)+1); % cLoc code sampled
at Fs

% --- Generate the incoming code with 3 periods of cLoc,
sample and shift
cIn = [cLoc cLoc cLoc];
k = 0:3*N-1;
cInSampled = cIn (floor (k*Rc/Fs) + 1); % cIn code sampled
at Fs

% --- Samples of the incoming code with a code-phase shift
Delay = 4*Fs/Rc;          % code Delay (samples)
cInSampledShift = circshift (cInSampled, [0 Delay]);

% --- Add AWGN noise
sigmaAWGN = 1;
% sigmaAWGN = 4;
% sigmaAWGN = 8;

cInSampledNoise = cInSampledShift + sigmaAWGN * randn (1,
3*N);

% --- Correlate the two sequences of samples
Corr = zeros (1, N);  % initialize the variable
for index = 0:N-1
   % --- correlate the codes
   Corr (index+1) = cInSampledNoise (1+index:N+index) *
   cLocSampled (1:N)';
end

% --- Plot correlation functions
xAxis = [0:(N-1)] ./Fs .* Rc;         % Prepare x-axis (chip)

figure,
plot (xAxis, Corr, '.-k'),
grid on
xlabel ('Delay (chip)')
ylabel ('Correlation')
```

```
title ('PRN code correlation')
axis tight
```

A.2 Example 2: Extension of Integration Time

The Matlab code reported below has been used to generate the figures in Example 23.2.

```
% --- clean up the environment
clear
close all
clc

% --- Variables definition
Rc = 0.5e6;             % Code Rate (chip/s)
Fs = 8e6;               % Sampling Frequency (Hz)

% --- define PRN codes
cLc = [1 -1 1 -1 -1 -1 -1 1 -1 ...
         1 -1 -1 -1 1 -1 -1 1 1 1 -1];

L = length (cLc);             % Code Length (chip)
N = floor (Fs*L/Rc);          % Code Length (samples)

% --- Sample the local code
k = 0:N-1;
cLocSampled = cLc (floor (k*Rc/Fs)+1); % cLoc code sampled
at Fs
% --- Number of sums for high sensitivity
Nsums = 10;
cLocSampled = repmat (cLocSampled, [1 Nsums]);

% - Generate the incoming code with M =20 periods of cLoc,
sample, and shift
M = 20;
cIn = repmat (cLc, [1 M]);
k = 0:M*N -1;
cInSampled = cIn (floor (k*Rc/Fs)+1);    % cIn code sampled @
Fs

% --- Samples of the incoming code with a code-phase
shift
Delay = 4*Fs/Rc;          % Code Delay (samples)
cInSampledShift = circshift (cInSampled, [0 Delay]);

% --- Add AWGN noise
sigmaAWGN = 1;
% sigmaAWGN = 12.5;
```

```
cInSampledNoise = cInSampledShift + sigmaAWGN * randn (1,
M*N);
%-------------------------------------------------------------------------

% --- Correlate the two sequences of samples
CorrFull = zeros (1, Nsums*N);    % initialize the variable
for index = 0:Nsums *N -1
    % --- correlate the codes
    CorrFull (index+1) = cInSampledNoise (1+index:2* N+
    index) * cLocSampled (1:2* N)';
end
% --- sum the correlation results
Corr = sum (reshape (CorrFull, N, Nsums)');

% --- Plot correlation functions
xAxis = [0:(N-1)] ./Fs .* Rc;          % Prepare x-axis (chip)

figure
plot (xAxis, Corr, '.-k')
grid on
xlabel ('Delay  (chip)')
ylabel ('Correlation')
title ('Code cross-correlation ')
axis tight
```

REFERENCES

[1] E. D. Kaplan and C. J. Hegarty, *Understanding GPS: principles and applications*. Artech House, 2006.

[2] P. Misra and P. Enge, *Global positioning system: signals, measurements and performance*. Massachusetts: Ganga-Jamuna Press, 2006.

[3] J. B. Y. Tsui, *Fundamentals of global positioning system receivers: a software approach*. Wiley-Interscience, 2005.

[4] F. S. T. Van Diggelen, *A-GPS: Assisted GPS, GNSS, and SBAS*. Artech House, 2009.

[5] US Air Force, "Navstar GPS space segment/navigation user interfaces," 2004.

[6] S. M. Kay, *Fundamentals of statistical signal processing*. Prentice Hall PTR, 1993.

[7] C. Strässle, D. Megnet, H. Mathis, and C. Bürgi, "The squaring-loss paradox," in *GNSS 20th International Technical Meeting of the Satellite Division*, 2007.

[8] D. Borio, "A statistical theory for GNSS signal acquisition," Ph.D. thesis, Politecnico di Torino, 2008.

[9] H. Elders-Boll and U. Dettmar, "Efficient differentially coherent code/Doppler acquisition of weak GPS signals," in *2004 IEEE Eighth International Symposium on Spread Spectrum Techniques and Applications*, pp. 731–735, IEEE, 2004.

[10] A. Schmid and A. Neubauer, "Performance evaluation of differential correlation for single shot measurement positioning," in *17th International Technical Meeting of the Satellite Division of the Institute of Navigation (ION GNSS 2004)*, pp. 1998–2009, 2001.

[11] W. Yu, B. Zheng, R. Watson, and G. Lachapelle, "Differential combining for acquiring weak GPS signals," *Signal Processing*, vol. 87, no. 5, pp. 824–840, 2007.

[12] F. Dovis and T. H. Ta, "High sensitivity techniques for GNSS signal acquisition," in *Global Navigation Satellite Systems: Signal, Theory and Applications*, InTech, 2012.

[13] R. Garello, L. Lo Presti, G. E. Corazza, and J. Samson, "Peer-to-peer cooperative positioning part i: GNSS aided acquisition," *INSIDE GNSS*, no. March, pp. 55–63, 2012.

AU: Publisher city needed

AU: Publisher city needed

Publisher city needed for all book citations throughout

AU: Is the issue number of this journal "March"? If not, could you provide the issue number?

AU: Is this an edited volume? If so, could you provide the editor?

[14] N. Linty, L. Musumeci, and F. Dovis, "Assistance requirements definition for GNSS receivers in hostile environments," in *2014 International Conference on Localization and GNSS (ICL-GNSS 2014)*, Piscataway, NJ, pp. 1–6, June 2014.
[15] D. Borio, L. Camoriano, and L. Lo Presti, "Impact of GPS acquisition strategy on decision probabilities," *IEEE Transactions on Aerospace and Electronic Systems*, vol. 44, pp. 996–1011, July 2008.
[16] P. Silva, H. Lopes, T. Peres, J. Silva, J. Ospina, F. Cichocki, F. Dovis, L. Musumeci, D. Serant, T. Calmettes, I. Pessina, and J. Perelló, "Weak GNSS signal navigation to the Moon," in *26th International Technical Meeting of The Satellite Division of the Institute of Navigation (ION GNSS+ 2013)*, pp. 3357–3367, 2013.
[17] N. Sokolova, D. Borio, B. Forssell, and G. Lachapelle, "Doppler rate measurements in standard and high sensitivity GPS receivers: Theoretical analysis and comparison," in *2010 International Conference on Indoor Positioning and Indoor Navigation (IPIN)*, pp. 1–9, September 2010.
[18] D. A. Shnidman, "The calculation of the probability of detection and the generalized Marcum Q-function," *IEEE Transactions on Information Theory*, vol. 35, no. 2, pp. 389–400, 1989.
[19] E. Falletti, D. Margaria, M. Nicola, G. Povero, and M. Gamba, "N-FUELS and SOPRANO: Educational tools for simulation, analysis and processing of satellite navigation signals," in *Frontiers in Education Conference, FIE*, pp. 303–308, 2013.
[20] P. L. Kazemi and C. O'Driscoll, "Comparison of assisted and stand-alone methods for increasing coherent integration time for weak GPS signal tracking," in *ION GNSS*, pp. 1730–1740, 2008.
[21] D. Borio and G. Lachapelle, "A non-coherent architecture for GNSS digital tracking loops," *annals of telecommunications-annales des télécommunications*, vol. 64, no. 9–10, pp. 601–614, 2009.
[22] D. Borio, N. Sokolova, and G. Lachapelle, "Memory discriminators for non-coherent integration in GNSS tracking loops," in *European Navigation Conference (ENC 2009)*, vol. 9, 2009.
[23] S. Stephens and J. Thomas, "Controlled-root formulation for digital phase-locked loops," *IEEE Transactions on Aerospace and Electronic Systems*, vol. 31, no. 1, pp. 78–95, 1995.
[24] N. Kassabian, "Design of pilot channel tracking loop systems for high sensitivity Galileo receivers" Ph.D. thesis, Politecnico di Torino, 2014.

AU: Is there a page range for this citation?